AIAA 91-1550

Progress on Multidimensional Upwind Euler Solvers for Unstructured Grids

R. Struijs, H. Deconinck and P. de Palma
Von Karman Institute for Fluid Dynamics
Waterloose Steenweg 72, 1640 St.-Genesius-Rode, Belgium

P. Roe and K.G. Powell
University of Michigan
Ann Arbor, Michigan, USA

10th Computational Fluid Dynamics Conference

June 24-26, 1991/Honolulu, Hawai

PROGRESS ON MULTIDIMENSIONAL UPWIND EULER SOLVERS FOR UNSTRUCTURED GRIDS.

R. Struijs, H. Deconinck and P. De Palma †,
Von Karman Institute for Fluid Dynamics,
Waterloose steenweg 72, 1640 Sint-Genesius-Rode, Belgium.

P.L. Roe and K.G. Powell,
University of Michigan,
Ann Arbor, Michigan, USA.

Abstract

In this paper we report on recent developments concerning multidimensional upwind schemes for solving the Euler equations on a grid composed of triangles. As a guideline we take the three concepts which constitute Roe's one dimensional approximate Riemann solver: (1) an analytic eigenvector- or wave decomposition of the flux derivative; (2) a discrete counterpart using a conservative linearization of the flux difference over a cell; (3) an upwind distribution of the decomposed parts over the meshpoints according to the sign of the corresponding eigenvalues. Each of these three elements are generalized for multidimensional flow, avoiding a dimension by dimension analysis. Eigenvector decompositions for the two dimensional flux divergence (two-dimensional wave models) have been proposed in 1986. A discrete counterpart using a recently developed conservative linearization of the flux balance over a triangle is explained in more detail. Nonlinear positive and linearity preserving scalar upwind distribution schemes are described for the distribution of the decomposed parts. Numerical results on standard subsonic, transonic and supersonic test cases are presented for different combinations of decomposition and scalar distribution schemes on triangulated meshes. Although many of the theoretical and numerical alternatives are still open, these results indicate that the present approach is a viable generalization of the one dimensional Riemann solvers.

1. Introduction

Over recent years, it has become increasingly apparent that the lack of truly multidimensional concepts is severely limiting the progress in, and performance of Euler- and Navier-Stokes computations[1-14]. State of the art upwind methods for compressible flow are based on Riemann solvers for the one dimensional Euler equations. Considering Roe's one dimensional flux difference splitter, the following distinct steps can be recognized in an interpretation which differs from the usual viewpoint in the sense that no reference is made to Riemann problems or the finite volume approach[15] :

1. First, derive an eigenvector decomposition of the one dimensional flux derivative. This eigenvector decomposition is in fact a wave pattern recognition step, decomposing a global perturbation in three simple wave contributions. Denoting by $\mathbf{U}$ the vector of conservative variables with flux vector $\mathbf{F}(\mathbf{U})$, the gradients are written as :

$$\begin{aligned} \frac{\partial \mathbf{U}}{\partial x} &= \sum_{k=1}^{3} \mathbf{r}^k \frac{\partial W^k}{\partial x} = \sum_{k=1}^{3} \alpha^k \mathbf{r}^k \\ \frac{\partial \mathbf{F}}{\partial x} &= \sum_{k=1}^{3} \lambda^k \mathbf{r}^k \frac{\partial W^k}{\partial x} = \sum_{k=1}^{3} \lambda^k \alpha^k \mathbf{r}^k \end{aligned} \tag{1.1}$$

where $\lambda^k(\mathbf{U})$ and $\mathbf{r}^k(\mathbf{U})$ are the eigenvalues and right eigenvectors of $A(\mathbf{U})$, the Jacobian matrix containing the derivatives of the flux vector with respect to the conservative variables.

The governing equation for each simple wave is

$$\frac{\partial W^k}{\partial t} + \lambda^k \frac{\partial W^k}{\partial x} = 0 \tag{1.2}$$

where W^k are the characteristic variables corresponding to entropy and two acoustic variables. The waves are traveling with speeds $\lambda^k \vec{1}_x$ along the x-axis, and have a strength α^k uniquely determined from

$$\alpha^k = \frac{\partial W^k}{\partial x} = \mathbf{l}^k \frac{\partial \mathbf{U}}{\partial x} \tag{1.3}$$

where $\mathbf{l}^k$ are the left eigenvectors of A such that

$$\mathbf{r}^k \mathbf{l}^m = \delta_{km} \tag{1.4}$$

with δ_{km} the Kronecker symbol. It is important to realize that in one dimension uniqueness and existence of this decomposition is guaranteed by the hyperbolicity of the system.

† presently at the University of Bari, Italy

2. In the second step, a discrete counterpart for eqs. (1.1) is constructed, commonly known as a flux difference splitter, although a more appropriate naming would be a flux balance or flux residual splitter, as will be seen later.

The flux residual is defined as the contour integral of the flux vector over a discrete cell representing two adjacent positions ($x_L < x_R$) on a mesh, with unknowns $\mathbf{U}_L$ and $\mathbf{U}_R$,

$$\int_{x_L}^{x_R} \frac{\partial \mathbf{U}}{\partial x} dx = \mathbf{U}_R - \mathbf{U}_L = \sum_{k=1}^{3} \widehat{\alpha^k \mathbf{r}^k}(\mathbf{U}_L, \mathbf{U}_R) \quad (1.5)$$

$$\int_{x_L}^{x_R} \frac{\partial \mathbf{F}}{\partial x} dx = \mathbf{F}_R - \mathbf{F}_L = \sum_{k=1}^{3} \widehat{\lambda^k \alpha^k \mathbf{r}^k}(\mathbf{U}_L, \mathbf{U}_R) \quad (1.6)$$

where the wave strength is computed from a discrete version of eq. (1.3).

$$\widehat{\alpha^k} = \overline{\mathbf{l}^k}(\mathbf{U}_L, \mathbf{U}_R)\,(\mathbf{U}_R - \mathbf{U}_L) \quad (1.7)$$

Eqs. (1.5) - (1.7) define what is called a conservative linearization, since it decomposes the conservative residual in scalar wave contributions related to the quasilinear form of the equations.

Roe showed[17] that such a conservative linearization is easily found by introduction of a new variable called the parameter vector $\mathbf{Z} = \sqrt{\rho}(1, u, H)^T$. With $\mathbf{Z}$ as the primary unknown, the linearization is simply given by

$$\begin{aligned} \overline{\mathbf{r}^k}(\mathbf{U}_L, \mathbf{U}_R) &= \mathbf{r}^k(\overline{\mathbf{Z}}) \\ \overline{\mathbf{l}^k}(\mathbf{U}_L, \mathbf{U}_R) &= \mathbf{l}^k(\overline{\mathbf{Z}}) \\ \overline{\lambda^k}(\mathbf{U}_L, \mathbf{U}_R) &= \lambda^k(\overline{\mathbf{Z}}) \end{aligned} \quad (1.8)$$

defining in this way the averaged Jacobian $\overline{A}(\mathbf{U}_L, \mathbf{U}_R) = A(\overline{\mathbf{Z}})$. Here, $\overline{\mathbf{Z}}$ is defined as

$$\overline{\mathbf{Z}} = \frac{1}{2}(\mathbf{Z}_L + \mathbf{Z}_R) \quad (1.9)$$

In the state $\overline{\mathbf{Z}}$, the primitive variables are given by

$$\overline{\mathbf{V}} = \mathbf{V}(\overline{\mathbf{Z}}) = \begin{pmatrix} \overline{\rho} \\ \overline{u} \\ \overline{H} \end{pmatrix} = \begin{pmatrix} \left[\frac{(\sqrt{\rho_L} + \sqrt{\rho_R})}{2}\right]^2 \\ \frac{u_L\sqrt{\rho_L} + u_R\sqrt{\rho_R}}{\sqrt{\rho_L} + \sqrt{\rho_R}} \\ \frac{H_L\sqrt{\rho_L} + H_R\sqrt{\rho_R}}{\sqrt{\rho_L} + \sqrt{\rho_R}} \end{pmatrix} \quad (1.10)$$

Combining eqs. (1.5) - (1.8) leads to the familiar result

$$\mathbf{F}_R - \mathbf{F}_L = A(\overline{\mathbf{Z}})(\mathbf{U}_R - \mathbf{U}_L) \quad (1.11)$$

Eqs. (1.5) - (1.7) have the important property that whenever $\mathbf{U}_L, \mathbf{U}_R$ are such that they can be connected by a single shockwave or a single contact discontinuity with speed s, only one non-vanishing term in the expansion remains, and eq. (1.6) reduces to the Rankine-Hugoniot jump relations, with $\overline{\lambda^k}$ the speed of the discontinuity.

By construction, the linearization of eq. (1.8) satisfies the following properties, additional to eq. (1.11) :

$$\overline{A}(\mathbf{U}, \mathbf{U}) = A(\mathbf{U}) \qquad \text{(consistency)} \quad (1.12)$$

$$\overline{A}(\mathbf{U}_L, \mathbf{U}_R) \qquad \text{has real eigenvalues and a complete set of linearly independent eigenvectors} \quad (1.13)$$

Eqs. (1.11), (1.12) and (1.13) are collectively referred to[17] as Property U, and ensure uniform validity of the linearization both in smooth flow and near discontinuities.

3. In the third step, a scalar upwind distribution scheme is applied to each part of the decomposed flux residual[16] given by eq. (1.6), depending on the orientation of the corresponding speed $\overline{\lambda^k}\vec{\mathbf{l}}_x$. For example, in the classical first order upwind scheme, the terms $\widehat{\lambda^k \alpha^k \mathbf{r}^k}$ corresponding to $\overline{\lambda^k} \geq 0$ are used to update $\mathbf{U}_R$, while the parts corresponding to $\overline{\lambda^k} \leq 0$ are used to update $\mathbf{U}_L$. Other schemes like Lax-Wendroff or Fromm's scheme can be recovered by selecting other distribution coefficients[15]. The key observation is that the problem is reduced to the design of accurate and oscillation free schemes for a scalar advection equation of type (1.2). Notice that the flux balance in the form of the LHS of eq. (1.6) is never needed in the distribution step. Due to the conservative linearization, the RHS of eq. (1.6) in the form of a sum of waves can be used, avoiding the evaluation of fluxes.

The three steps described above constitute the familiar Roe's approximate Riemann solver in terms which are suited for generalization to two and three space dimensions without resorting to a dimension by dimension analysis :

1. In two or three space dimensions, the decomposition of the divergence of the flux vector will be written as a sum of terms of the form eigenvectors × wavespeed × wavestrength, just like eqs. (1.1). The decomposition however is not uniquely determined as in one space dimension, and intrinsic flow properties will be used to find out which eigenvectors, speeds and corresponding directions are relevant. Two dimensional wave decompositions which generalize eqs. (1.1) have been introduced already around 1986, when Roe[1] and Deconinck et al[2] came up with criteria to detect and select relevant simple wave patterns given a linearized flow field. Both decompositions are summarized, used and compared in the present work. A new variant of Roe's approach[18] is recapitulated in section 2.

2. Eq. (1.6) generalizes to a contour integral around a two dimensional or three dimensional cell. On these elements, a conservative linearization can be constructed having Property U. This conservative linearization which was recently developed[19], forms an essential part of the multi dimensional solver and will be discussed in section 3. Key requirement is the use of triangular cells in two dimensions and tetrahedra in three dimensions. These elements are the natural extensions of the one dimensional line element, permitting the definition of a unique linear variation of the unknown over the cell for given data at the vertices. This again indicates that truly multidimensional extensions differ strongly from the dimension by dimension analysis, in which quadrilateral cells are the natural two dimensional extension of a line segment.

3. Scalar distribution schemes will distribute the decomposed parts of the flux balance to the vertices of the cell, depending on the orientation of the corresponding advection speed in the two dimensional or three dimensional

space. The schemes discussed will meet constraints concerning conservation, positivity and accuracy as explained in section 4.

Each one of these three constitutive steps of the multidimensional generalization of Roe's one dimensional flux difference splitter is a topic in itself, deserving a more elaborate discussion than this paper permits. In fact, progress on wave models[1,2,18,20], linearization[19,24] and discretization[21,22,23,24] has been reported in various publications over the last five years, showing an evolution of understanding and sophistication. Although research in the above topics continues, we think that the basic concepts at the root of the method are understood and fit together very well. Not excluding further developments we present in this paper for the first time a coherent description which may later be refined or extended, but which is not likely to be drastically changed. Furthermore, we show numerical results with the method, where in previous publications[14,18] the essential element of the conservative linearization[19] was missing.

The multidimensional generalization treated in this paper is in strong contrast with the classically adopted dimension by dimension generalization of the one dimensional approximate Riemann solver. In the standard interpretation in a finite volume context, the flux at the interface between x_L and x_R can be found from the solution of the approximate Riemann problem for the linearized equation

$$\frac{\partial U}{\partial t} + A(\overline{\mathbf{Z}})\frac{\partial \mathbf{U}}{\partial x} = 0$$

$$\mathbf{U}(x,0) = \mathbf{U}_L \quad , \quad x \leq 0$$

$$\mathbf{U}(x,0) = \mathbf{U}_R \quad , \quad x > 0$$

where $\mathbf{U}_L$ and $\mathbf{U}_R$ are either the average state in adjacent cells or some higher order reconstruction at the cell interface. Consequently the waves emanating from the jump of the unknowns at the cell interface influence the value of the unknowns of the neighbouring cells $\mathbf{U}_L$ and $\mathbf{U}_R$.

In two or more space dimensions, the flux at a cell interface is defined in exactly the same one dimensional way. The flux jacobian is now taken in the direction of the cell face normal $\vec{n}_{LR}$. Again, the waves influence only $\mathbf{U}_L$ and $\mathbf{U}_R$. The standard generalization has the drawback that a set of Riemann problems is solved related to each cell face. Every flux is decomposed in waves traveling normal to the cell face, which is irrelevant from the physical point of view. This results is a solution algorithm which depends on geometrical variables which have little or no relation with the relevant flow directions. Consequently the choice of the grid has a disproportional influence on the solution, as has been observed e.g. for calculations in which a shear (contact discontinuity) or shock is present in the solution, but where these phenomena are not aligned with the grid.

The multidimensional generalization discussed in this paper does not have this shortcoming. The wave propagation directions depend uniquely on intrinsic flow properties, while the scalar discretization schemes aim at a discretization along these preferential directions.

As an intermediate step between the approach followed in this paper and the dimensionally split approach, so-called Rotated Riemann Solvers can be considered[6-13]. For the definition of the cell face Riemann problem they take into account variables like flow direction or velocity difference direction over a cell face. In this way some multidimensional behaviour is introduced. Although some promising results have been obtained along these lines, this is not the approach followed in this work. Instead we prefer to abandon the finite volume viewpoint which inevitably leads to some one dimensional Riemann problem between two neighbouring cell states, and we adopt the residual distribution strategy as introduced before[16,21,24,25].

Test computations indicate that the choice of the wave decomposition is very important and is still a matter of further research. Indeed, satisfactory results were only obtained for one of the 6 wave models (model C), while the 4 wave model failed completely for subsonic and transonic flow. Another topic for further investigation is the implementation of boundary conditions in the multidimensional upwind solver. Nevertheless, comparison of the computations using model C with standard grid aligned upwind solvers indicates that non-aligned discontinuities are indeed captured in fewer cells by the present approach.

2. Multidimensional wave decomposition models for the Euler equations.

The generalization of Roe's one dimensional scheme, as decribed in the introduction, requires first an eigenvector decomposition of the two dimensional flux divergence, similar to what has been achieved in one dimension by eq. (1.1). Two approaches have been proposed in the past. One is based on two dimensional characteristic theory [2,3,5], and the other is based on a superposition of simple wave solutions[1,20,18].

In the first approach, 4 particular compatibility equations are selected, and the corresponding eigenvectors are used to split the flux divergence. The decomposition takes the form

$$\frac{\partial \mathbf{F}}{\partial x} + \frac{\partial \mathbf{G}}{\partial y} = \sum_{k=1}^{4} \lambda^k \, \alpha^k \, \mathbf{r}^k + \mathbf{S} \qquad (2.1)$$

The 4 eigenvectors are selected to minimize in some sense the term $\mathbf{S}$, but elimination of this term is not always possible. Moreover the computation of the relevant wave directions requires the solution of a quadratic equation, introducing a non-uniqueness problem.

In the second approach[1,20,18], at least for the models considered in this paper, 6 simple wave solutions are selected such that their superposed effect is equivalent to the flux divergence. Thus the 6 eigenvectors, strengths and speeds are found analytically. The decomposition is always complete and unique, given by

$$\frac{\partial \mathbf{F}}{\partial x} + \frac{\partial \mathbf{G}}{\partial y} = \sum_{k=1}^{6} \lambda^k \, \alpha^k \, \mathbf{r}^k \qquad (2.2)$$

Both decompositions are briefly described below, but the emphasis is put on the second because it has lead to more satisfactory results at this stage of our research, as will be discussed in section 5.

2.1 Characteristic decomposition model.

Deconinck and Hirsch[2] proposed a decomposition method in which characteristic compatibility equations are selected which lead to an optimal decoupling of the Euler equations into a set of scalar 2D convection equations. Starting point is the system of Euler equations in divergence form,

$$\frac{\partial \mathbf{U}}{\partial t} + \frac{\partial \mathbf{F}}{\partial x} + \frac{\partial \mathbf{G}}{\partial y} = 0 \ , \quad \text{or} \quad \frac{\partial \mathbf{U}}{\partial t} + \vec{\nabla} \cdot \vec{\mathbf{F}} = 0 \qquad (2.3)$$

with $\mathbf{U} = (\rho, \rho u, \rho v, \rho E)^T$. Characteristic variables $\mathbf{W}$ are defined by a transformation using a 4×4 matrix L [2-5] :

$$\begin{aligned} \partial \mathbf{U} &= L^{-1} \partial \mathbf{W} & \partial \mathbf{W} &= L \partial \mathbf{U} \\ L^{-1} &= (\mathbf{r}^1, \mathbf{r}^2, \mathbf{r}^3, \mathbf{r}^4) & L &= (\mathbf{l}^1, \mathbf{l}^2, \mathbf{l}^3, \mathbf{l}^4)^T \end{aligned} \qquad (2.4)$$

The column vectors $\mathbf{r}^k$ and row vectors $\mathbf{l}^k$ are right, respectively left eigenvectors of the Jacobians of eq. (2.3) in some particular flow dependent directions. In vector notation, the transformed system representing four particular characteristic compatibility equations becomes

$$\frac{\partial \mathbf{W}}{\partial t} + D_x \frac{\partial \mathbf{W}}{\partial x} + D_y \frac{\partial \mathbf{W}}{\partial y} + \mathbf{Q} = 0 \qquad (2.5)$$

where D_x and D_y are diagonal matrices, which have as diagonal elements the convection speeds in x respectively y direction. The terms $\mathbf{Q}$ represent off diagonal terms, which appear since in general the Jacobians of the fluxes $\mathbf{F}$ and $\mathbf{G}$ do not commute. The different terms in eq. (2.5) are given by :

$$\partial \mathbf{W} = \begin{pmatrix} \partial \rho - \frac{1}{c^2} \partial p \\ \vec{s}^{(1)} \cdot \partial \vec{u} \\ \vec{\kappa}^{(2)} \partial \vec{u} + \frac{1}{\rho c} \partial p \\ -\vec{\kappa}^{(2)} \partial \vec{u} + \frac{1}{\rho c} \partial p \end{pmatrix} \qquad (2.6a)$$

$$D_x = \begin{pmatrix} u & & & \\ & u & & \\ & & u + c\kappa_x^{(2)} & \\ & & & u - c\kappa_x^{(2)} \end{pmatrix} \qquad D_y = \begin{pmatrix} v & & & \\ & v & & \\ & & v + c\kappa_y^{(2)} & \\ & & & v - c\kappa_y^{(2)} \end{pmatrix} \qquad (2.6b)$$

$$\mathbf{Q} = \begin{pmatrix} 0 \\ \frac{1}{\rho} s_x^{(1)} \partial_x p + s_y^{(1)} \partial_y p \\ c s_x^{(2)} (s_x^{(2)} \partial_x u + s_y^{(2)} \partial_x v) + c s_y^{(2)} (s_x^{(2)} \partial_y u + s_y^{(2)} \partial_y v) \\ c s_x^{(2)} (s_x^{(2)} \partial_x u + s_y^{(2)} \partial_x v) + c s_y^{(2)} (s_x^{(2)} \partial_y u + s_y^{(2)} \partial_y v) \end{pmatrix} \qquad (2.6c)$$

The convection speeds for the four characteristic components are therefore

$$\vec{\lambda}^{(1)} = \vec{u}, \quad \vec{\lambda}^{(2)} = \vec{u}, \quad \vec{\lambda}^{(3)} = \vec{u} + c\vec{\kappa}^{(2)}, \quad \vec{\lambda}^{(4)} = \vec{u} - c\vec{\kappa}^{(2)}. \qquad (2.7)$$

The vectors $\vec{s}^{(1)}$ and $\vec{s}^{(2)}$ are normal to the vectors $\vec{\kappa}^{(1)}$ respectively $\vec{\kappa}^{(2)}$. The selection of the optimal characteristics is done by choosing two normals $\vec{\kappa}^{(1)}$ and $\vec{\kappa}^{(2)}$ which render the transformation optimal in the sense that the coupling term $\mathbf{Q}$ is minimized. The first decomposition normal $\vec{\kappa}^{(1)}$ is therefore chosen parallel to the pressure gradient, while the second decomposition normal $\vec{\kappa}^{(2)}$ is a function of the strain rate tensor. More details on the decomposition can be found in the original paper[2] and[3,4,5].

Note that both normals and hence the decomposition are a function of gradients of the flow variables only, and do not depend on any direction dictated by the mesh. Transforming eq. (2.5) back to conservative variables, one obtains the decomposition of the flux divergence, eq. (2.1), where

$$\alpha^k = \frac{\vec{\lambda}^k}{\lambda^k} \cdot \vec{\nabla} \mathbf{W}^k \qquad (2.8)$$

$$\lambda^k = |\vec{\lambda}^k| \qquad (2.9)$$

$$\mathbf{S} = \sum_{k=1}^{4} Q^k \mathbf{r}^k \qquad (2.10)$$

2.2 The six wave models.

This decomposition proposed by Roe[2,20] is based on a superposition of 6 simple wave solutions, assuming linearized flow. Simple wave solutions for linearized flow are defined by

$$\mathbf{U}^k = W^k \mathbf{r}^k = \alpha^k \mathbf{r}^k \cdot (x n_x + y n_y - \lambda_n^k t) \qquad (2.11)$$

where α^k is the strength of the wave, $n_x = \cos\theta$ and $n_y = \sin\theta$ the components of the unit vector $\vec{n}$ in the propagation direction θ (omitting superscript k), and $\mathbf{r}^k$ a right eigenvector of the Jacobian $An_x + Bn_y$ with corresponding eigenvalue λ_n^k. The gradient of $\mathbf{U}^k$ is

$$\vec{\nabla} \mathbf{U}^k = \alpha^k \vec{n} \, \mathbf{r}^k \qquad \alpha^k = |\vec{\nabla} W^k| \qquad (2.12)$$

$$\vec{\nabla} W^k = |\vec{\nabla} W^k| \vec{n} = \alpha^k \vec{n} = \mathbf{l}^k \vec{\nabla} \mathbf{U}^k \qquad (2.13)$$

Substitution in the Euler equations shows that the characteristic variable W^k satisfies the advection equation

$$\frac{\partial W^k}{\partial t} \mathbf{r}^k + (An_x + Bn_y) |\vec{\nabla} W^k| \mathbf{r}^k = 0 \qquad (2.14)$$

or

$$\frac{\partial W^k}{\partial t} + \vec{\lambda}_n^k \cdot \vec{\nabla} W^k = 0 \qquad (2.15)$$

where the two dimensional advection speed vector $\vec{\lambda}_n^k$ has been introduced,

$$\vec{\lambda}_n^k = \lambda_n^k \vec{n} \qquad (2.16)$$

Eq. (2.15) is the two-dimensional equivalent for the simple wave equation in one dimension, eq. (1.2). In eq. (2.15), the speed $\vec{\lambda}_n^k$ is in the direction of the gradient $\vec{\nabla} W^k$ and is therefore called the 'gradient dependent speed'. For the Euler equations, these speeds are obtained for a given direction $\vec{n}$ by solving the eigenvalues of $An_x + Bn_y$, leading to

$$\begin{aligned} \vec{\lambda}_n^{1,2} &= (\vec{u} \cdot \vec{n}) \vec{n} \\ \vec{\lambda}_n^{3,4} &= (\vec{u} \cdot \vec{n} \pm c) \vec{n} \end{aligned} \qquad (2.17)$$

The first two correspond to an entropy and a shear wave, while the second two correspond to two acoustic waves (fig.

1). For subsonic flow in the direction $\vec{n}, (\vec{u} \cdot \vec{n} < c)$, λ_n^3 and λ_n^4 have opposite signs, while for supersonic flow in the direction $\vec{n}$ they have the same sign.

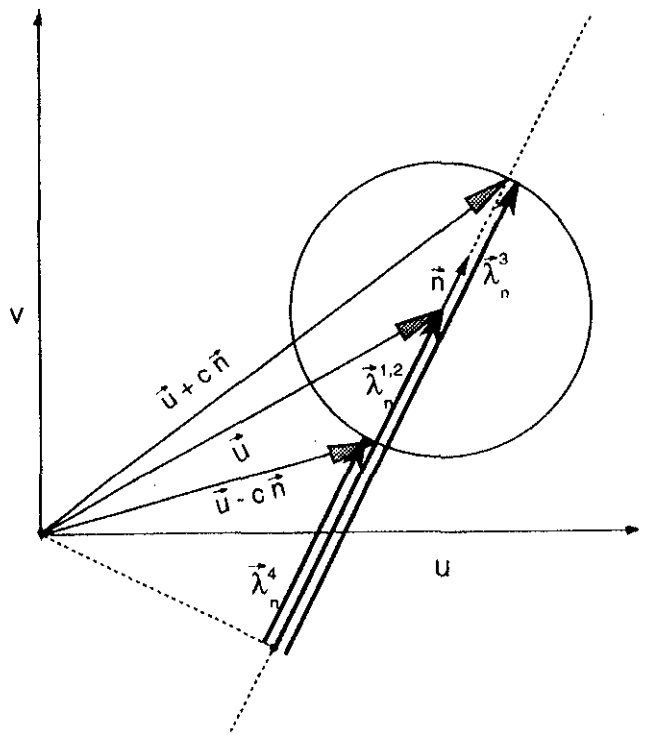

Fig. 1. Speeds and directions for the waves in the 6 wave model.

The speeds (2.17) are quite different from the linearized speeds obtained from the characteristic wave decomposition, eq. (2.7). However, looking at eq. (2.15) one observes that the space operator is unaffected if we replace $\vec{\lambda}_n^k$ by $\vec{\lambda}^k$, where $\vec{\lambda}^k$ is defined such that it satisfies

$$\vec{\lambda}_n^k = (\vec{\lambda}^k \cdot \vec{n})\vec{n} \tag{2.18}$$

because

$$\vec{\lambda}_n^k \cdot \vec{\nabla} W^k = (\vec{\lambda}^k \cdot \vec{n})\, \vec{n} \cdot \vec{\nabla} W^k = (\vec{\lambda}^k \cdot \vec{n}) |\vec{\nabla} W^k| = \vec{\lambda}^k \cdot \vec{\nabla} W^k \tag{2.19}$$

Hence for the Euler equations, one can construct the linearized speeds $\vec{\lambda}^k$ as

$$\begin{aligned} \vec{\lambda}^{1,2} &= \vec{u} \\ \vec{\lambda}^{3,4} &= \vec{u} \pm c\vec{n} \end{aligned} \tag{2.20}$$

which are precisely the speeds used in the characteristic decomposition model, where $\vec{\kappa}^{(1)}, \vec{\kappa}^{(2)}$ play the role of $\vec{n}$.

Matching the local gradient with a superposition of simple waves of the above type uniquely defines the decomposition, precisely as in 1D, eq. (1.1.a).

In one dimension there is only one degree of freedom per wave, namely its strength α^k. The basis consists of 3 independent eigenvectors, which means that in total 3 strengths have to be found. On the other hand, the space derivative of the flux has 3 components. The flux derivatives can therefore be uniquely matched to this basis of eigenvectors.

In two dimensions each simple wave has two degrees of freedom, namely its strength α^k and its propagation direction θ^k. Now the basis consists of 4 independent eigenvectors, so in total 4 strengths and 4 angles have to be found. The space derivative of the flux has now 4 components, while the derivatives are in x and y direction. Again the flow derivatives can be matched to this basis of 4 eigenvectors. The complex algebra which comes out of this matching process can be considerably reduced by adding two acoustic waves, in which case some of the strengths and angles have to be specified a priori. This option has been taken by Roe[1,20] in his 6 wave model, where by physical reasoning some of the directions are fixed. The choice of waves for what Roe called model B, is :

(1) One entropy wave with unknown direction ψ_s and intensity S_s : two unknowns.
(2) A shear wave with unknown strength S_e traveling in the direction perpendicular to the streamlines.
(3) Four mutually perpendicular acoustic waves, contributing five unknowns : one direction θ and four strengths α_i, $i = 1, 4$.

The choice of the direction of the shear wave leaves some room for discussion. Comparing the linearized speeds (2.20) with the characteristic speeds (2.7) both approaches lead to the same shear wave treatment if the shearwave direction in the 6 wave model is selected parallel with the pressure gradient direction ($\vec{\kappa}^{(1)}$). This was proposed by De Palma et al[18] (model C) and decouples the shear wave from the pressure disturbances. Model C shows indeed improved performance compared to model B (see section 5).

It is clear that many other wave models may be proposed, based on physical reasoning, and it is likely that more performant models will come out of ongoing research in this field. In any case, superposing a number of waves to match the gradients leads to

$$\vec{\nabla}\mathbf{U} = \sum_k \alpha^k \vec{n}\, \mathbf{r}^k = \sum_k \vec{\nabla} W^k \mathbf{r}^k \tag{2.22}$$

After substitution in the flux divergence one obtains expression (2.2), which can also be written as

$$\begin{aligned} \frac{\partial \mathbf{F}}{\partial x} + \frac{\partial \mathbf{G}}{\partial y} &= \sum_k \vec{\lambda}_n^k \, \vec{\nabla}\mathbf{W}^k \mathbf{r}^k \\ &= \sum_k \vec{\lambda}^k \, \vec{\nabla}\mathbf{W}^k \mathbf{r}^k \end{aligned} \tag{2.23}$$

because of the equivalence (2.19).

3. Multidimensional linearization with property U

The second step in a multidimensional generalization of Roe's approximate Riemann solver is the construction of a discrete counterpart of the wave decomposition (2.1) or (2.2), to be called the flux residual or flux balance splitter, by analogy to the flux difference splitter in 1D. Such a discrete form is obtained after integrating (2.1) or (2.2) over a cell. The LHS then becomes a flux integration in conservation form, whereas the RHS should decompose it

in linearized scalar wave contributions. An essential ingredient in this proces is the use of a conservative linearization procedure[19]

It will be shown that a consistent conservative discretisation can easily be obtained starting from the condition that U varies linearly over the cell. In one dimension a cell is simply a line element. Given the value of the unknown U at the cell interfaces, the solution can be represented by a piecewise linear function in between. The two dimensional cells having the property of linearly varying unknowns are triangles, and in three dimensions tetrahedra, with the unknowns given at the vertices. This representation is identical to standard linear finite element conventions.

The aim now is to write multidimensional generalizations for the discrete form of the gradient of the unknowns as given in the previous section, and of the divergence of the flux on a triangle. In other words, eqs. (2.1) or (2.2), depending on the choice of the wave model, has to be written in a form similar to eqs. (1.5) and (1.6). The linearization has to satisfy the two dimensional equivalent of Property U (eqs. (1.11), (1.12) and (1.13)).

Let us first define the discrete derivative of a variable over a triangle as the average:

$$\widehat{\vec{\nabla} q} = \frac{1}{S_T} \iint \vec{\nabla} q(x,y) dS = \frac{1}{S_T} \oint q \vec{n} dl \qquad (3.1)$$

with S_T the area of the triangle. Only for linear space variation of q, this leads to the simple formula (see section 4) :

$$\widehat{\vec{\nabla} q} = \frac{1}{2\, S_T} \sum_{i=1}^{3} \vec{n_i} q_i \qquad (3.2)$$

where $\vec{n_i}$ is the scaled inward normal opposite to vertex i with value q_i.

For the derivative $\frac{\partial \widehat{\mathbf{F}}}{\partial x}$ we can write

$$S_T \frac{\partial \widehat{\mathbf{F}}}{\partial x} = \iint \frac{\partial \mathbf{F(U)}}{\partial x} dS = \iint A(\mathbf{U}) \frac{\partial \mathbf{U}}{\partial \mathbf{x}} dS \qquad (3.3)$$

At this point it is evident why the choice of linearly varying unknown U over the cell is made : for a linearly varying U, the gradient $\vec{\nabla}\mathbf{U}$ is constant over the cell, and can be taken out of the integration in the RHS of eq. (3.3) :

$$\iint \frac{\partial \mathbf{F(U)}}{\partial x} dS = \left[\iint A(\mathbf{U}) dS \right] \frac{\partial \widehat{\mathbf{U}}}{\partial x} \qquad (3.4)$$

which enables us to define a linearized Jacobian

$$\overline{A}(\mathbf{U}_1, \mathbf{U}_2, \mathbf{U}_3) = \frac{1}{S_T} \iint A(\mathbf{U}) dS \qquad (3.5)$$

with $\mathbf{U}_1, \mathbf{U}_2, \mathbf{U}_3$ the values of U at the vertices of the triangle. Hence, merely assuming linear variation of U leads to an exact evaluation of the flux contour integral over a triangle, provided eq. (3.5) can be integrated analytically, thus satisfying our requirement for Property U. Two-dimensional extensions of eqs. (1.13) and (1.14) are fulfilled, while the two dimensional generalization of eq. (1.11) is written as :

$$\widehat{\vec{\nabla} \cdot \vec{\mathbf{F}}} = \overline{A} \frac{\partial \widehat{\mathbf{U}}}{\partial \mathbf{x}} + \overline{B} \frac{\partial \widehat{\mathbf{U}}}{\partial \mathbf{y}} \qquad (3.6)$$

where $\overline{B}$ is obtained in a similar way as $\overline{A}$.

The straightforward choice of taking the conservative variables as independent linearly varying unknowns is not the best to be made. Due to the fact that $A(\mathbf{U})$ and $B(\mathbf{U})$ are strongly nonlinear in U, the integration needed in (3.5) is hopelessly cumbersome to compute.

A much more convenient choice is the parameter vector $\mathbf{Z} = (z_1, z_2, z_3, z_4)^T = \sqrt{\rho}(1, u, v, H)^T$, defined by Roe[17]. The reason is that each component of $\mathbf{U}, \mathbf{F}$ and G is merely a bilinear function of the components of Z, and as a consequence $\frac{\partial \mathbf{U}}{\partial \mathbf{Z}}$, $\frac{\partial \mathbf{F}}{\partial \mathbf{Z}} = A_Z$ and $\frac{\partial \mathbf{G}}{\partial \mathbf{Z}} = B_Z$ are just linear functions in the components of Z. Therefore, integration over the triangle reduces to taking the arithmetic mean, e.g.:

$$\overline{A}_Z = \frac{1}{S_T} \iint_T A_Z(\mathbf{Z}) dS = A_Z \left(\frac{\mathbf{Z}_1 + \mathbf{Z}_2 + \mathbf{Z}_3}{3} \right) = A_Z(\overline{\mathbf{Z}}) \qquad (3.7)$$

and similarly $\overline{B}_Z = B_Z(\overline{\mathbf{Z}})$, where $\overline{\mathbf{Z}}$ is a 2D generalization of the Roe average[17] :

$$\overline{\mathbf{Z}} = \left(\frac{\mathbf{Z}_1 + \mathbf{Z}_2 + \mathbf{Z}_3}{3} \right) = \frac{1}{3} \begin{pmatrix} \sqrt{\rho}_1 + \sqrt{\rho}_2 + \sqrt{\rho}_3 \\ u_1\sqrt{\rho}_1 + u_2\sqrt{\rho}_2 + u_3\sqrt{\rho}_3 \\ v_1\sqrt{\rho}_1 + v_2\sqrt{\rho}_2 + v_3\sqrt{\rho}_3 \\ H_1\sqrt{\rho}_1 + H_2\sqrt{\rho}_2 + H_3\sqrt{\rho}_3 \end{pmatrix} \qquad (3.8)$$

Primitive variables V in the state $\overline{\mathbf{Z}}$ is given by

$$\overline{\mathbf{V}} = \begin{pmatrix} \overline{\rho} \\ \overline{u} \\ \overline{v} \\ \overline{H} \end{pmatrix} = \begin{pmatrix} \frac{(\sqrt{\rho}_1 + \sqrt{\rho}_2 + \sqrt{\rho}_3)^2}{9} \\ \frac{u_1\sqrt{\rho}_1 + u_2\sqrt{\rho}_2 + u_3\sqrt{\rho}_3}{\sqrt{\rho}_1 + \sqrt{\rho}_2 + \sqrt{\rho}_3} \\ \frac{v_1\sqrt{\rho}_1 + v_2\sqrt{\rho}_2 + v_3\sqrt{\rho}_3}{\sqrt{\rho}_1 + \sqrt{\rho}_2 + \sqrt{\rho}_3} \\ \frac{H_1\sqrt{\rho}_1 + H_2\sqrt{\rho}_2 + H_3\sqrt{\rho}_3}{\sqrt{\rho}_1 + \sqrt{\rho}_2 + \sqrt{\rho}_3} \end{pmatrix} \qquad (3.9)$$

Note that the multidimensional conservative linearization depends on all unknowns U in the cell. This is in contrast with the linearization used in the dimension by dimension generalization, where only the values adjacent to a cell interface are used. Also the use of triangles is crucial for the simplicity in the above reasoning.

Given linear variation of Z, we define the linearized Jacobian in conservative variables, $\overline{A}$, such that:

$$\begin{aligned} \iint_{S_T} \frac{\partial \mathbf{F(Z)}}{\partial x} dS &= \overline{A} \iint_{S_T} \frac{\partial \mathbf{U(Z)}}{\partial x} dS \\ &= \overline{A} \left[\iint_{S_T} \frac{\partial \mathbf{U}}{\partial \mathbf{Z}} dS \right] \frac{\partial \widehat{\mathbf{Z}}}{\partial x} \end{aligned} \qquad (3.10)$$

while at the same time

$$\iint_{S_T} \frac{\partial \mathbf{F(Z)}}{\partial x} dS = \overline{A}_Z \frac{\partial \widehat{\mathbf{Z}}}{\partial x} S_T \qquad (3.11)$$

The matrix $M_Z(\mathbf{Z}) = \frac{\partial \mathbf{U(Z)}}{\partial \mathbf{Z}}$ needed in (3.10) is again a linear function of Z. It is given as[24]

$$M_Z(\mathbf{Z}) = \begin{pmatrix} 2z^1 & 0 & 0 & 0 \\ z^2 & z^1 & 0 & 0 \\ z^3 & 0 & z^1 & 0 \\ \frac{1}{\gamma}z^4 & \frac{\gamma-1}{\gamma}z^2 & \frac{\gamma-1}{\gamma}z^3 & \frac{1}{\gamma}z^1 \end{pmatrix} \tag{3.12}$$

Hence, its integration over the triangle is given by

$$\overline{M}_Z = \frac{1}{S_T}\iint_{S_T} M_Z(\mathbf{Z})dS = M_Z(\overline{\mathbf{Z}}) \tag{3.13}$$

Substituting in (3.10) and identification with (3.11) leads to

$$\overline{A}\cdot\overline{M}_Z = \overline{A}_Z \qquad \text{and similarly} \qquad \overline{B}\cdot\overline{M}_Z = \overline{B}_Z \tag{3.14}$$

An important consequence is the following : since $\overline{A}\cdot M_Z(\overline{\mathbf{Z}}) = A_Z(\overline{\mathbf{Z}})$, one has

$$\overline{A} = A_Z(\overline{\mathbf{Z}})\cdot M_Z^{-1}(\overline{\mathbf{Z}}) = \frac{\partial\mathbf{F}}{\partial\mathbf{Z}}\frac{\partial\mathbf{Z}}{\partial\mathbf{U}}\bigg|_{Z=\overline{Z}} = \frac{\partial\mathbf{F}}{\partial\mathbf{U}}\bigg|_{Z=\overline{Z}} = A(\overline{\mathbf{Z}}) \tag{3.15}$$

This means that consistent averages are now easily obtained for any of the matrices. For example, for the primitive variable $\mathbf{V} = (\rho, u, v, p)^T$ [24], it is easy to check that

$$\frac{\partial\mathbf{V}}{\partial\mathbf{Z}} = \begin{pmatrix} 2z^1 & 0 & 0 & 0 \\ -\frac{z^2}{(z^1)^2} & \frac{1}{z^1} & 0 & 0 \\ -\frac{z^3}{(z^1)^2} & 0 & \frac{1}{z^1} & 0 \\ \frac{\gamma-1}{\gamma}z^4 & \frac{-\gamma-1}{\gamma}z^2 & -\frac{\gamma-1}{\gamma}z^3 & \frac{\gamma-1}{\gamma}z^1 \end{pmatrix} \tag{3.16}$$

Hence, the consistent computation of the derivatives $\widehat{\vec{\nabla}\mathbf{V}}$ in primitive variables is given by :

$$\begin{pmatrix} \widehat{\vec{\nabla}\rho} \\ \widehat{\vec{\nabla}u} \\ \widehat{\vec{\nabla}v} \\ \widehat{\vec{\nabla}p} \end{pmatrix} = \begin{pmatrix} 2\sqrt{\overline{\rho}}\,\vec{\nabla}\sqrt{\rho} \\ \frac{1}{\sqrt{\overline{\rho}}}[\vec{\nabla}\sqrt{\rho}u - \overline{u}\vec{\nabla}\sqrt{\rho}] \\ \frac{1}{\sqrt{\overline{\rho}}}[\vec{\nabla}\sqrt{\rho}v - \overline{v}\vec{\nabla}\sqrt{\rho}] \\ \frac{\gamma-1}{\gamma}\sqrt{\overline{\rho}}[\overline{H}\vec{\nabla}\sqrt{\rho} - \overline{u}\vec{\nabla}\sqrt{\rho}u - \overline{v}\vec{\nabla}\sqrt{\rho}v + \vec{\nabla}\sqrt{\rho}H] \end{pmatrix} \tag{3.17}$$

where $\overline{\rho}, \overline{u}, \overline{v}$ and $\overline{H}$ are given by (3.9). Clearly, these gradients are consistent in the sense that if ρ, u, v or p are constant over the cell, then their gradient is zero (note that $p = \frac{\gamma-1}{\gamma}\rho[H - \frac{u^2+v^2}{2}]$). Further, they are defined constant over a cell since the gradients of the parameter variable in the RHS are constants. In this way, the residual (3.6) can be expressed in any variable, e.g. in $\mathbf{V}$:

$$\frac{\partial\widehat{\mathbf{F}}}{\partial x} + \frac{\partial\widehat{\mathbf{G}}}{\partial y} = \overline{A}_V\frac{\partial\widehat{\mathbf{V}}}{\partial x} + \overline{B}_V\frac{\partial\widehat{\mathbf{V}}}{\partial y} \tag{3.18}$$

where $\widehat{\vec{\nabla}\mathbf{V}}$ has to be computed from (3.17), and

$$\overline{A}_V = \frac{\partial\mathbf{F}}{\partial\mathbf{V}}(\overline{\mathbf{V}}) \quad , \quad \overline{B}_V = \frac{\partial\mathbf{G}}{\partial\mathbf{V}}(\overline{\mathbf{V}}) \tag{3.19}$$

It should be well realized that the gradients in the LHS of eq. (3.17) are evaluated in the way of eq. (3.1). However, one cannot use eq. (3.2) since the primitive variables do not vary linearly over the triangle following the choice of the parameter vector as independent variable. If we look at the 1D expression for $\widehat{\Delta u}$ for simplicity, writing out the 1D counterpart of eq. (3.17) for $\widehat{\Delta u}$ reveals that $\widehat{\Delta u} = \frac{\tilde{\rho}}{\rho}\cdot(u_R - u_L)$. The term $\tilde{\rho} = \sqrt{\rho_L\rho_R}$ appearing in the difference is the Roe average density, which is distinctly different from the averaged density appearing in eq. (1.10). In fact, the average $\tilde{\rho}$ is an average which is mainly used to evaluate expressions like $\Delta(\rho u)$ in terms of arbitrary differences $\Delta\rho = \rho_R - \rho_L$ and $\Delta u = u_R - u_L$ rather than in terms of $\widehat{\Delta\rho}$ and $\widehat{\Delta u}$. In either one of the conventions, the result looks very similar :

$$\Delta(\rho u) = \tilde{\rho}\,\Delta u + \tilde{u}\,\Delta\rho = \overline{\rho}\,\widehat{\Delta u} + \overline{u}\,\widehat{\Delta\rho}$$

where $\tilde{u} = \overline{u}$.

3.1 Conservative linearization applied to the characteristic decomposition.

It is now straightforward to apply the results from the preceding section to the decomposition described in section 2.1. Indeed, one can evaluate the strengths (eq. 2.8) as :

$$\widehat{\alpha^k} = \frac{\overline{\vec{\lambda}^k}}{\overline{\lambda^k}}\widehat{\vec{\nabla}W^k} \tag{3.20}$$

where:

$$\widehat{\vec{\nabla}W^k} = \overline{l^k}\,\widehat{\vec{\nabla}\mathbf{U}} \tag{3.21}$$

while the coupling term $\mathbf{S}$ of eq. (2.10) is evaluated from:

$$\widehat{\mathbf{S}} = \sum_{k=1}^{4}\widehat{Q^k}\,\overline{\mathbf{r}^k} \tag{3.22}$$

with $\widehat{Q^k}$ obtained from (2.6c), using the linearized variables and the gradients in primitive variables (eq. (3.17)). The final result is a conservative splitting of the flux balance over a triangle of the form

$$\oint_{S_T}\vec{\mathbf{F}}\vec{n}dl = \iint_{S_T}\left(\frac{\partial\mathbf{F}}{\partial x} + \frac{\partial\mathbf{G}}{\partial y}\right)dS = S_T\left[\sum_{k=1}^{4}\overline{\lambda^k}\,\widehat{\alpha^k}\,\overline{\mathbf{r}^k} + \widehat{\mathbf{S}}\right] \tag{3.23}$$

3.2 Conservative linearization applied to 6 wave models.

The basic equation matching the wave strengths with the gradients[8] is performed in primitive variables $\mathbf{V} = (\rho, u, v, p)^T$, using :

$$\widehat{\vec{\nabla}\mathbf{V}} = \sum_{1}^{6}\widehat{\alpha^k}\vec{n}^k\overline{\tilde{\mathbf{r}}^k} \tag{3.24}$$

Here, the LHS is given by eq. (3.17), where $\overline{\tilde{\mathbf{r}}^k}$ are the right eigenvectors in primitive variables, linearized using the parameter variable average.

Once the angles and the strengths are obtained from the matching (3.24), the conservative flux balance is obtained from:

$$\iint_{S_T}\left(\frac{\partial\mathbf{F}}{\partial x} + \frac{\partial\mathbf{G}}{\partial y}\right)dS = S_T\sum_{k=1}^{6}\overline{\lambda^k}\,\widehat{\alpha^k}\,\overline{\mathbf{r}^k} \tag{3.25}$$

which can as well be written as, eq. (2.2) :

$$\iint_{S_T} \left(\frac{\partial \mathbf{F}}{\partial x} + \frac{\partial \mathbf{G}}{\partial y}\right) dS = S_T \sum_{k=1}^{6} \overline{\vec{\lambda}^k} \; \widehat{\vec{\nabla} W^k} \; \overline{\mathbf{r}^k} \qquad (3.26)$$

or

$$\iint_{S_T} \left(\frac{\partial \mathbf{F}}{\partial x} + \frac{\partial \mathbf{G}}{\partial y}\right) dS = S_T \sum_{k=1}^{6} \overline{\vec{\lambda}_n^k} \; \widehat{\vec{\nabla} W^k} \; \overline{\mathbf{r}^k} \qquad (3.27)$$

where

$$\begin{aligned} \widehat{\vec{\nabla} W^k} &= \widehat{\alpha^k \vec{n}^k} \\ \overline{\vec{\lambda}_n^k} &= (\overline{\vec{\lambda}^k} \cdot \vec{n}^k)\vec{n}^k \end{aligned} \qquad (3.28)$$

It is remarkable that in the numerical implementation, conservative fluxes are never estimated. Indeed, because of the conservative linearization it is sufficient to compute directly each of the terms in the RHS, and to distribute them to the vertices of the triangles using one of the scalar distribution schemes discussed in the next section.

Even more, it is not necessary to compute the residual in conservative variables as in eqs. (3.25) - (3.27). One can use any quasilinear form of the Euler equations, e.g. using $\mathbf{V} = (\rho, u, v, p)^T$ as dependent variable :

$$\frac{\partial \mathbf{V}}{\partial t} + \tilde{A}\frac{\partial \mathbf{V}}{\partial x} + \tilde{B}\frac{\partial \mathbf{V}}{\partial y} = 0 \qquad (3.29)$$

where $\tilde{A}$ and $\tilde{B}$ are the jacobians of the Euler equations taking $\mathbf{V}$ as the independent varable.

In this variable, $\tilde{A}$ and $\tilde{B}$ have a very simple form[5], and so have the eigenvectors $\tilde{\mathbf{r}}^k$.

The residual in the quasilinear form is then computed as

$$\iint_{S_T} \left(\tilde{A}\frac{\partial \mathbf{V}}{\partial x} + \tilde{B}\frac{\partial \mathbf{V}}{\partial y}\right) dS = S_T \sum_{k=1}^{6} \overline{\lambda^k} \; \widehat{\alpha^k} \; \overline{\tilde{\mathbf{r}}^k} \qquad (3.30)$$

and the updating will be done in primitive variable $\mathbf{V}$. This has actually not been implemented for the numerical results presented in section 5, but it will certainly improve the efficiency of the approach.

4. Scalar advection schemes.

The first two steps of the multi-dimensional generalization of Roe's approximate Riemann solver , sections 2 and 3, resulted in the representation of the flux divergence or residual over a cell as the superposition of contributions with known speed and orientation. In the characteristic decomposition method we have 4 characteristic contributions with known orientation, together with a term representing pure diffusion, which can be handled with a central discretization. Alternatively, in the 6 wave models we have just 6 waves with given speed, strength and orientation. Using a conservative linearization procedure, the discrete formulation of these waves has been found in terms of the unknowns at the vertices of a triangular cell. The upwind discretization of the convective terms in the splitting therefore only has to deal with each component seperately, governed by a linear scalar advection equation, e.g. eq. (2.5) for the characteristic decomposition or eq. (2.15) for the 6 wave model, which taking into account eq. (2.19) can be written as

$$\frac{\partial W^k}{\partial t} + \vec{\lambda}^k \cdot \vec{\nabla} W^k = 0 \qquad k = 1,6 \qquad (4.1)$$

where by construction of the linearization

$$\vec{\lambda}^k \cdot \vec{\nabla} W^k = \vec{\lambda}^k \cdot \alpha^k \vec{n}^k \qquad (4.2)$$

As a result of the representation as a sum of waves, the numerical behaviour of the discretized system is completey governed by the schemes for the two-dimensional scalar wave equation, concerning accuracy, convergence, stability and monotonicity. This explains the increased interest in the solution of the scalar advection equation. Any inperfection in the scalar schemes will show up in the Euler results, and we may not expect the results for the system of equations to be better than the performance for the scalar equation. In the results section, some elementary test cases show that the solution of the system is of about the same quality as for the scalar wave equation in the case of model C decomposition.

A general theory of scalar advection schemes is presented in a separate paper at this conference[9], based on the pioneering work[21] which was later elaborated[24,25]. In the present section we confine ourselves to a description of the two residual distribution schemes used for the computations presented in section 5. The first scheme is the optimal linear positive scheme on a compact stencil composed of the vertices of all triangles meeting at a given meshpoint. It has been proven that such a linear positive scheme is at most first order accurate in space. Therefore a second nonlinear variant has been developed which is both positive and second order accurate in space (for a homogeneous advection equation), very similar to the nonlinear TVD schemes in one dimension.

4.1. Preliminaries

Consider the numerical solution of the two-dimensional scalar advection equation

$$W_t + \vec{\lambda} \cdot \vec{\nabla} W = 0 \qquad (4.3)$$

where $\vec{\lambda}$ is a constant vector in the 2D plane. The mesh is taken as an arbitrary triangulation of the domain. Over a typical triangle T with vertices V_1, V_2, V_3, and edges E_1, E_2, E_3 (see fig. 2), the solution is represented as piecewise linear. The integral of W_t over element T will be

$$\iint_{S_T} W_t \, dx \, dy = \iint_{S_T} \vec{\lambda} \cdot \vec{\nabla} W \, dx \, dy = \oint_{\partial T} W \vec{\lambda} \cdot d\vec{n} \qquad (4.4)$$

Here ∂T is the boundary and S_T the area of T, and Gauss' theorem has been used. Note that $d\vec{n}$ is the inward normal to an element of the boundary. Since W varies linearly within each triangle, and hence along each side, (4.4) becomes

$$\phi_T = \frac{1}{2}(W_1 + W_2)\vec{\lambda}\cdot\vec{n}_3 + \frac{1}{2}(W_2 + W_3)\vec{\lambda}\cdot\vec{n}_1 + \\ + \frac{1}{2}(W_3 + W_1)\vec{\lambda}\cdot\vec{n}_2 \qquad (4.5)$$

where $\vec{n}_1$ is the inward normal to E_1 scaled with the length of E_1, and so on. Rearranging, one obtains

$$\phi_T = -\frac{1}{2}\sum_{i=1}^{3} W_i\,\vec{\lambda}\cdot\vec{n}_i \qquad (4.6)$$

where the last change is possible because for any triangle,

$$\vec{n}_1 + \vec{n}_2 + \vec{n}_3 = \vec{0} \qquad (4.7)$$

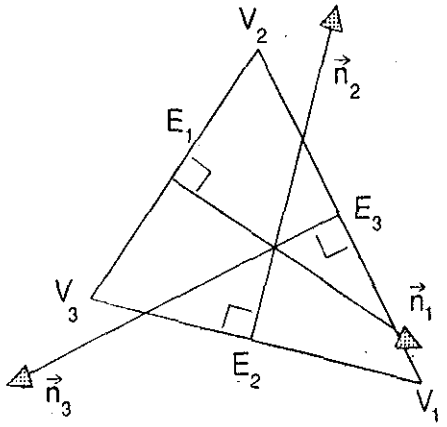

Fig. 2. Notation to describe a general triangle with edges E_1, vertices V_i and normals $\vec{n}_i$ scaled with the length of E_i.

Note that if $\vec{\lambda}\cdot\vec{n}_i$ is positive, then flow enters T through E_i, and vice versa. Because of (4.7), we can write many alternative formulae for ϕ_T. Some of these are

$$\phi_T = -\frac{\vec{\lambda}\cdot\vec{n}_1}{2}(W_1 - W_3) - \frac{\vec{\lambda}\cdot\vec{n}_2}{2}(W_2 - W_3) \\ -\frac{\vec{\lambda}\cdot\vec{n}_2}{2}(W_2 - W_1) - \frac{\vec{\lambda}\cdot\vec{n}_3}{2}(W_3 - W_1) \qquad (4.8) \\ = -\frac{\vec{\lambda}\cdot\vec{n}_3}{2}(W_3 - W_2) - \frac{\vec{\lambda}\cdot\vec{n}_1}{2}(W_1 - W_2)$$

The existence of these alternatives will prove useful. An alternative route into these results would have been the interesting identity (cfr. eq. (3.2))

$$2\,S_T\vec{\nabla}W = \sum_{1}^{3} W_i\vec{n}_i \qquad (4.9)$$

The natural analogue of the scalar distribution scheme in one dimension as discussed in the introduction would appear to be the following. For each triangle in turn carry out, for $i = 1, 2, 3$, the following three replacements,

$$S_iW_i \;\rightarrow\; S_iW_i + \alpha_i^T\Delta t\phi_T \qquad (4.10)$$

where S_i is the area that weights W_i in the integration of W. It will be one-third the total area of the triangles having i as a vertex, commonly known as the median dual cell around i, see fig. 3. It can easily be shown [21,24,25] that (4.10) is a conservative scheme, provided

$$\sum_{1}^{3}\alpha_i^T = 1 \qquad \forall T \qquad (4.11)$$

All schemes discussed will satisfy this condition.

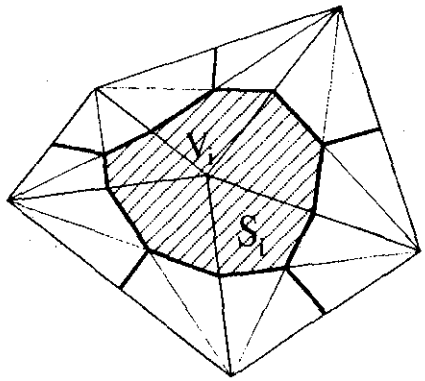

Fig. 3. Median dual cell around vertex i.

If a given triangle sends only contributions to its own vertices (which is the only choice considered in this work), the schemes have a compact stencil for a given meshpoint i, which contains at most the vertices of all triangles with common vertex i. This restriction is, moreover, an aid to efficient coding. After assembling the contributions from all triangles T meeting in i, we obtain the scheme

$$W_i^{n+1} = W_i^n + \frac{\Delta t}{S_i}\sum_{T}\alpha_i^T\phi_T \qquad (4.12)$$

or

$$W_i^{n+1} = W_i^n - \frac{\Delta t}{S_i}\sum_{T}\alpha_i^T\sum_{j=1}^{3}\frac{\vec{\lambda}\cdot\vec{n}_j^T}{2}W_{T_j} \qquad (4.13)$$

with T_1, T_2, and T_3 the vertices of T and $\vec{n}_j^T$ the normal opposite to vertex T_j in triangle T.

Additional to constraint (4.11) for a conservative scheme, we consider the following two design criteria :

Property P : Positivity

Positivity[26] means that every new value W_i^{n+1} can be written as a convex combination of old values :

$$W_i^{n+1} = \sum_{k} c_kW_k^n \quad \text{with} \quad \forall c_k \geq 0, \qquad (4.14)$$

while $\sum c_k = 1$ for consistency. It guarantees a maximum principle for the discrete steady state solution thus prohibiting the occurrence of new extrema and imposing stability on the explicit scheme (4.13).

As far as we know, this condition has never been put forward in the finite element context. In the finite differ-

ence and finite volume context it is well known and extensively used to design discontinuity capturing high resolution schemes, even on unstructured grids. A stronger condition but easier to verify is local positivity by which it is required that the contribution of each triangle separately is positive[24].

Property LP : Linearity Preservation

By this we require that the scheme preserves the exact steady state solution whenever this is a linear function of the space coordinates x and y, for any arbitrary triangulation of the domain. Since the condition considers only the steady state, it is an accuracy requirement on the space discretization only.

In the context of linear finite elements property LP is an obvious requirement, but since our methods originate from a different approach it is not automatically enforced, as will be seen in the following. It includes consistency in space defined as preservation of an exact constant steady state. Indeed, there is a strong relation between the notion of constancy preservation and first order accuracy of finite difference space discretizations on regular grids at one hand, and linearity preservation versus second order accuracy on the other hand. In fact this equivalence is the basis for the well known MUSCL interpretation of upwind differencing on regular grids and it has been shown that schemes satisfying LP are second order on a uniform Cartesian grid, at least for the homogeneous advection equation.

It has been shown in[24,25] that linear schemes (c_k constant in eq. (4.14)) cannot be positive and linearity preserving at the same time, thus generalizing Godunov's theorem on the incompatibility between second order accuracy and monotonicity preservation. Hence, to combine both properties P and LP, one has to look for nonlinear schemes, precisely as in 1D with the TVD schemes. Before introducing a nonlinear scheme which satisfies both properties P and LP, we discuss the optimal linear scheme.

4.2. The optimal linear scheme satisfying property P (positivity)

The scheme is called the N-scheme, the nomenclature of Sidilkover[27] for schemes on structured grids. For a triangle with one inflow side (fig. 4), with downstream vertex 3, the straightforward choice is to send the entire fluctuation to the downstream node 3, giving $\alpha_1^T = \alpha_2^T = 0, \alpha_3^T = 1$ and for the updating of node 3 due to triangle T:

$$W_3^{n+1} = W_3^n - \frac{\Delta t}{S_3}\left[\frac{\vec{\lambda}\cdot\vec{n}_1}{2}(W_1 - W_3) + \frac{\vec{\lambda}\cdot\vec{n}_2}{2}(W_2 - W_3)\right] \tag{4.15}$$

where the form (4.8) has been used. Since both $\vec{\lambda}\cdot\vec{n}_1$ and $\vec{\lambda}\cdot\vec{n}_2$ are negative, this leads to a locally positive scheme under the condition

$$\Delta t < \frac{S_3}{\frac{1}{2}\vec{\lambda}\cdot\vec{n}_3} \tag{4.16}$$

On the other hand, this update is linearity preserving as well, since the updating vanishes for an exact linear solution. Hence for one inflow side triangles, the one target distribution to the downstream node satisfies both P and LP2, and it is the optimal choice[24].

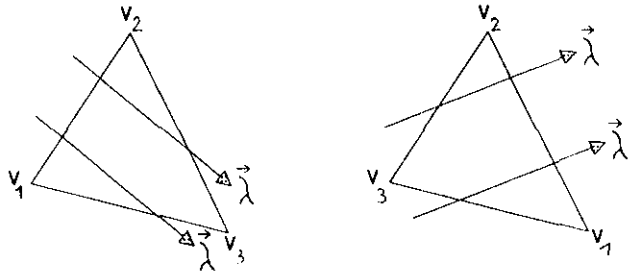

Fig. 4. Examples of a triangle with either one or two inflow sides.

$(a) : \vec{\lambda}\cdot\vec{n}_1 > 0, \vec{\lambda}\cdot\vec{n}_2 < 0, \vec{\lambda}\cdot\vec{n}_3 < 0$

$(b) : \vec{\lambda}\cdot\vec{n}_1 > 0, \vec{\lambda}\cdot\vec{n}_2 > 0, \vec{\lambda}\cdot\vec{n}_3 < 0$

Consider now the second case of a two inflow side triangle and suppose that two sides, say E_1, E_2 are both inflow sides (fig. 4). The upwind philosophy suggests that no signal is sent to V_3. In[24,25] it is then shown that the following update from triangle T is optimal :

$$\begin{aligned} S_1 W_1^{n+1} &= S_1 W_1^n - \Delta t[\frac{\vec{\lambda}\cdot\vec{n}_1}{2}(W_1^n - W_3^n)] \\ S_2 W_2^{n+1} &= S_2 W_2^n - \Delta t[\frac{\vec{\lambda}\cdot\vec{n}_2}{2}(W_2^n - W_3^n)] \end{aligned} \tag{4.17}$$

In constructing this scheme, we have again used the alternative expression (4.8). Local positivity of the scheme (4.17) is obtained, taking into account that both $\vec{\lambda}\cdot\vec{n}_1$ and $\vec{\lambda}\cdot\vec{n}_2$ are positive coefficients, if the timestep is limited by

$$\Delta t \leq \min\left[\frac{S_1}{\left(\frac{1}{2}\vec{\lambda}\cdot\vec{n}_1\right)}, \frac{S_2}{\left(\frac{1}{2}\vec{\lambda}\cdot\vec{n}_2\right)}\right] \tag{4.18}$$

A less restrictive condition for global positivity is obtained by taking into account the coefficients of W_P for all triangles T meeting at P leading to

$$\Delta t \leq \frac{S_P}{\sum_T \max\left(0, \frac{1}{2}\vec{\lambda}\cdot\vec{n}_P^T\right)} \tag{4.19}$$

Of all linear positive schemes, the scheme (4.15), (4.17) is the one which allows the maximum timestep and has the most narrow stencil (hence its name N-scheme where N stands for Narrow). In many cases, namely if only 3 triangles contribute to a given vertex, it leads to a 3-point stencil.

Therefore it is not surprising that when applied to a Cartesian grid triangulated by tracing the diagonals such that their projection on $\vec{\lambda}$ is maximized, the N-scheme becomes identical to the optimal most compact linear positive scheme on a structured Cartesian grid, having a 3 point stencil and known as the streamline upwind scheme of Rice and Schnipke[28]. Sidilkover[27] renamed this scheme as the N-scheme, explaining our present nomenclature on unstructured grids. The scheme on a structured grid is well known to be first order accurate in space, confirming our findings that the N-scheme (as well as any other linear positive scheme) is not linearity preserving. When applied with

the "wrong" choice of the diagonals, the N-scheme becomes identical to regular dimensionally split first order upwinding, which is again the most compact 3-point stencil for that choice of the diagonal.

The N-scheme is also closely related to the work of Hughes et al[20] in the development of Petrov-Galerkin finite-element methods. They also found it necessary to distinguish between cases with one or two inflow sides, and gave a neat geometric construction that clarifies (4.17). The velocity $\vec{\lambda}$ is to be regarded, as in fig. 5, as the sum of components parallel to E_1 and E_2,

$$\vec{\lambda} = \vec{\lambda}_1 + \vec{\lambda}_2 \tag{4.20}$$

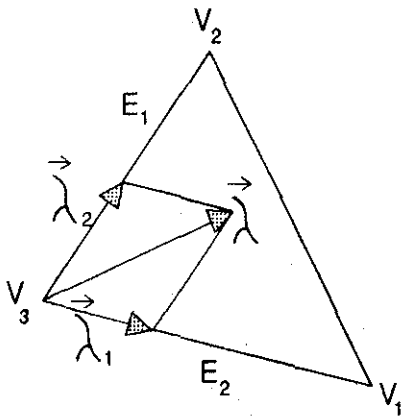

Fig. 5. The effect of convection speed vector $\vec{\lambda}$ as a sum of its components along sides 1 and 2.

The fluctuation due to $\vec{\lambda}_1$, is (cfr. 4.8)

$$\begin{aligned}\phi_1 &= -\frac{1}{2}(\vec{\lambda}_1.\vec{n}_1)(W_1 - W_3) - \frac{1}{2}(\vec{\lambda}_1.\vec{n}_2)(W_2 - W_3) \\ &= -\frac{1}{2}(\vec{\lambda}_1.\vec{n}_1)(W_1 - W_3) \\ &= -\frac{1}{2}(\vec{\lambda}.\vec{n}_1)(W_1 - W_3)\end{aligned} \tag{4.21}$$

and similarly the fluctuation due to $\vec{\lambda}_2$ is

$$\phi_2 = -\frac{\vec{\lambda}\cdot\vec{n}_2}{2}(W_2 - W_3) \tag{4.22}$$

Now the whole of ϕ_1 can be sent to V_1, because for $\vec{\lambda}_1$, only E_2 is an inflow side, and the whole of ϕ_2 can be sent to V_2.

Of course, the main drawback of the N scheme is that it does not preserve a linear steady state solution (property LP) as can be easily verified from eq. (4.17) : For an exact linear steady state, the sum of the two split parts adds to zero, but each of the parts seperately can be non-zero, thus sending an update which destroys the exact linear solution at the next time step.

4.3. The NN scheme.

Linear schemes satisfying property LP are important from the viewpoint of accuracy, although they lack the crucial property of positivity (P). Both central and upwind schemes belong to this class, with among the central schemes the well known Petrov Galerkin and Streamline Diffusion (or Least Squares) Petrov Galerkin Finite Element schemes, for which a Lax-Wendrov derivation has be given[24]. The numerical diffusion obtained with all these schemes is comparable, and as could be expected much lower than for any of the linear positive schemes we have developed. However, these schemes cannot be retained since they do not preserve monotonic profiles over discontinuities.

Instead, we consider a nonlinear scheme, called the NN scheme (Nonlinear Narrow), which is indeed positive and linearity preserving. Because of our generalized Godunov theorem, the scheme has necessarily to be nonlinear.

Consider again the linear N-scheme. For triangles with one inflow side, the updating (4.15) satisfies both property P and LP. So in this case there is no need at all to turn to a nonlinear scheme.

On the other hand, for a two inflow side triangle (fig. 4) with downstream vertices 1 and 2, the updating is given in eq. (4.17), and the scheme is positive under condition (4.18). However, this updating is not linearity preserving as mentioned before in the previous section: for this to be true, both terms $\frac{\vec{\lambda}\cdot\vec{n}_1}{2}(W_1^n - W_3^n)]$ and $\frac{\vec{\lambda}\cdot\vec{n}_2}{2}(W_2^n - W_3^n)]$ should vanish for an exact linear solution, while in reality only the sum of the two do vanish on a general triangulation.

To cure the problem, we may recall (section 2) that *the residual is not changed if one replaces $\vec{\lambda}$ by the gradient* dependent convection speed eq.(2.18), given by

$$\vec{\lambda}_n = (\vec{\lambda}\cdot\vec{n})\vec{n} \quad , \quad \vec{n} = \frac{\vec{\nabla}W}{|\vec{\nabla}W|} \tag{4.23}$$

where $\vec{n}$ is a unit vector parallel with $\vec{\nabla}W$ evaluated with eq. (4.9). Indeed, one easily verifies that

$$\vec{\lambda}_n\cdot\vec{\nabla}W = \vec{\lambda}\cdot\vec{\nabla}W \tag{4.24}$$

Also, one may add a component parallel to the isolines of W without changing the residual (fig. 6). For

$$\vec{\lambda}^* = \vec{\lambda}_n + \beta(\vec{\lambda} - \vec{\lambda}_n) \tag{4.25}$$

with β an arbitrary real, one still has

$$\vec{\lambda}^*\cdot\vec{\nabla}W = \vec{\lambda}\cdot\vec{\nabla}W \tag{4.26}$$

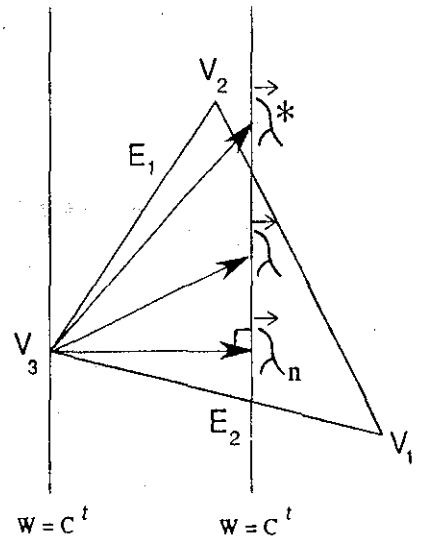

Fig. 6. The fluctuation remains unchanged if $\vec{\lambda}^*$ is chosen along the line perpendicular to $\vec{\lambda}_n$.

However, using $\vec{\lambda}_n$ or $\vec{\lambda}^*$ instead of $\vec{\lambda}$ makes the scheme non-linear, even for a linear equation. Choosing $\vec{\lambda}_n$ instead of $\vec{\lambda}$ in the distribution makes the scheme linearity preserving, because

$$\vec{\lambda}_n = (\vec{\lambda}\cdot\vec{\nabla}W)\cdot\frac{\vec{\nabla}W}{|\vec{\nabla}W|^2} = \frac{\Phi_T}{S_T}\frac{\vec{\nabla}W}{|\vec{\nabla}W|^2} \qquad (4.27)$$

vanishes for a steady state which is a linear function of x and y. Two cases may occur : if $\vec{\lambda}_n\cdot\vec{n}_1$ and $\vec{\lambda}_n\cdot\vec{n}_2$ are both positive, the resulting scheme

$$\begin{aligned} S_1W_1^{n+1} &= S_1W_1^n - \Delta t[\frac{\vec{\lambda}_n\cdot\vec{n}_1}{2}(W_1^n - W_3^n)] \\ S_2W_2^{n+1} &= S_2W_2^n - \Delta t[\frac{\vec{\lambda}_n\cdot\vec{n}_2}{2}(W_2^n - W_3^n)] \end{aligned} \qquad (4.28)$$

is positive as well (for Δt small enough). This situation corresponds to a location of $\vec{\lambda}_n$ pointing inside the triangle in the same way as $\vec{\lambda}$ (fig. 6). However, in the case that $\vec{\lambda}_n$ points outside the triangle, either $\vec{\lambda}_n\cdot\vec{n}_1$ or $\vec{\lambda}_n\cdot\vec{n}_2$ is negative and the resulting scheme is no longer positive. In fig. 7 this situation is depicted, for $\vec{\lambda}_n\cdot\vec{n}_1 < 0$ and $\vec{\lambda}_n\cdot\vec{n}_2 > 0$. Recalling that any $\vec{\lambda}^*$ defined in (4.25) can be used, we may select the smallest $\vec{\lambda}^*$ which makes the scheme positive, which is the vector with the direction along the edge E_1 (fig. 7). Since this makes the scheme single target to node 2, $\vec{\lambda}^*\cdot\vec{n}_1$ being zero, the scheme is indeed positive for Δt small enough.

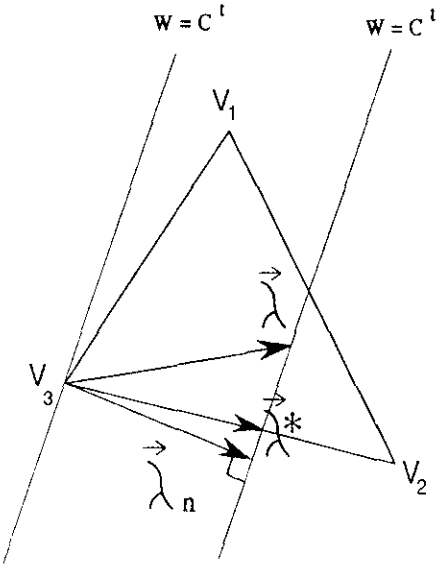

Fig. 7. Choice of convection direction for the distribution scheme if $\vec{\lambda}_n$ points outside the triangle.

Summarizing, the NN scheme which is both positive and linearity preserving, is given by the following algorithm.

1) if the triangle has one inflow side according to $\vec{\lambda}$, send the residual to the unique downstream vertex.
2) if the triangle is two target according to $\vec{\lambda}$, say with nodes 1 and 2, compute $\vec{\lambda}_n$
   - if both $\vec{\lambda}_n\cdot\vec{n}_2 > 0$ and $\vec{\lambda}_n\cdot\vec{n}_2 > 0$ use the two target formula (4.28).
   - else if $\vec{\lambda}_n\cdot\vec{n}_1 < 0$ and $\vec{\lambda}_n\cdot\vec{n}_2 > 0$ send the residual to node 2.
   - else send the residual to node 1

4.4 Application to the Euler equations.

Application of the above schemes to the Euler equations is very easy, considering each of the splitting parts as a scalar residual $\vec{\lambda}^k\cdot\vec{\nabla}W^k$ multiplied with right eigenvector $\mathbf{r}^k$.

N-scheme.

Considering the characteristic decomposition model, the 4 scalar contributions are distributed according to the N-scheme using the speeds $\vec{u}, \vec{u}, \vec{u}+c\vec{\kappa}^{(2)}$ and $\vec{u}-c\vec{\kappa}^{(2)}$. The source term $\mathbf{S}$, eq. (2.10) is distributed either by sending equal parts to the 3 nodes or by distributing $Q^k\mathbf{r}^k$ according to the speed $\vec{\lambda}^k$.

For the 6 wave model, the 6 scalar contributions are again distributed according to the speeds $\vec{\lambda}^k$ corresponding to each of the 6 waves, namely $\vec{u}, \vec{u}, \vec{u}\pm c\vec{n}$ and $\vec{u}\pm c\vec{n}_\perp$, where $\vec{n}$ is the propagation direction of the first acoustic wave, and $\vec{n}_\perp$ is perpendicular to $\vec{n}$.

NN-scheme.

In the NN-scheme, additional 'gradient dependent' advection speeds are computed for the two-target distributions.

For the 4 wave model ,these are given by eq. (2.18).

For the 6 wave models these 'gradient dependent' speeds are simply the original speeds resulting from the model as given in eq. (2.17).

From the above discussion it appears that the two approaches have become very similar with respect to the entropy and shear wave, the main difference being in the treatment of the acoustic waves.

Nevertheless, no results could be obtained with the 4 wave model, except for the supersonic oblique shock reflection problem. On the other hand, the 6 wave models, in particular model C has proven to be quite robust for all test cases considered so far, although some problems remain with respect to the solid wall boundary conditions.

4.5 Application to structured grids.

The linearization and spatial discretization described in this paper are based on triangulation of the domain, making use of a uniquely defined gradient of unknowns over a triangle. The most obvious domain of applications is therefore the area of unstructured solvers as indicated by the title of this paper.

For structured solvers however, the multidimensional generalization can be used as well. It is sufficient to divide a quadrilateral by one of its diagonals triangles, to be able to apply the method described so far. Question is of course, which diagonal has to be inserted to split the quadrilateral in to two triangles ? On a scalar equation it can be shown that taking the diagonal closest to the advection direction and applying the N scheme corresponds to the Rice and Schnipke scheme[28] on a Cartesian grid, while taking the other diagonal reduces to the much more diffusive standard finite volume upwinding on the quadrilateral cells. This behaviour is confirmed by numerical tests on scalar convection equations.

For a system of equations it would be ideal to take the optimal diagonal for each of the waves involved in modeling the flow. In doing so, no clear procedure is available yet to ensure conservation. We can for the moment only be conservative if we take the same diagonal for a given quadrilateral for all 4 or 6 waves. The choice of diagonal will be made by the wave with the largest strength α^k. We must pay attention to the normalization of the eigenvectors, since the choice of r^k in the evaluation of the residual is sensitive with respect to scaling. It turns out that the eigenvectors as defined by Roe permit the use of the strength without scaling.

Some results on a structured grid with optimization of the underlying triangles appear in section 5. For comparison, the choice of diagonal can be made independent of the solution. To avoid bias due to a certain choice of diagonal, diagonals can be arranged to alternate going from one quadrilateral to another. Some results on those isotropic grids appear also in section 5.

5. Results

The purpose of the present section is to show evidence that the methodology described in this paper represents a viable alternative for the well established dimensionally split (or locally 1D) TVD upwind solvers, especially on unstructured grids composed of triangles. For comparison with structured grid results, we use the approach of dividing quadrilaterals along one of their diagonals as described in section 4.5.

Many of the results shown cannot yet compete with standard TVD results, namely for subsonic and transonic flow test cases. For supersonic flow on the other hand, the present results indicate that shocks or contact discontinuities not aligned with the grid are resolved in fewer cells with the present approach, when compared with standard solvers on the same structured grid. For upwind solvers it is the subsonic flow which represents the most critical regime, due to the fact that the domain of dependence is omnidirectional, while the discretization only picks out a discrete number of privileged directions. Therefore, multidimensional upwind solvers have it very difficult to treat this situation correctly, and subsonic results have only been obtained after the consistent conservative linearization was introduced, (section 3.). Even with the correct linearization, no subsonic results have been obtained for the characteristic decomposition (section 2.1), for reasons which are not well understood at the moment. One of the problems might be the non uniqueness problem in determining the direction $\kappa^{(2)}$ in the decomposition or the incompleteness of the decoupling. Further investigation in this area is needed.

Another problem area to be further investigated is the implementation of consistent boundary conditions, especially along solid walls. It appears that there is a loss of conservation in the layer of triangles along the solid walls. Taking the symmetry boundary condition or doubling the oblique shock problem by adding the mirror problem to avoid a solid wall boundary condition gave no improvement.

The following test cases are considered :

a) Reflection of an oblique shock on a flat plate, with an incoming Mach number of 2.9 and an incident shock angle of 29^0.

b) Channel flow with a 4% bump with inlet Mach number of 1.4 (mainly supersonic).

c) Channel flow with a 4.2% bump for inlet Mach numbers of 0.6 (c1, fully subsonic) and 0.85 (c2, transonic).

Some of the test cases have also been run with a standard state of the art grid aligned finite volume Roe flux difference splitter by M. Manna[32] on a quadrilateral grid, using minmod limited MUSCL extrapolation and κ-schemes with $\kappa = 1/3$ in a cell-centered formulation.

The unstructured grids were generated with an advancing front method combined with Delauney triangulation. The user only specifies the point distribution at the boundaries. This program was written by J.D. Müller at VKI and Ann Arbour. The resulting grids can be highly regular, many of the triangles being equilateral and about of the same size if the boundary point distribution is smooth enough. For the plotting on the unstructured grid use was made of software written by P. Vankeirsbilck.

The oblique shock test case has been chosen to make comparisons between different wave models, discretization schemes, and for the structured solver the choice of underlying triangles.

Results on an unstructured grid are shown in fig. 8 where the solution in the form of iso Mach lines is superimposed on the grid. For this computation the NN scheme with model C has been used. The corresponding iso entropy lines are given in fig. 9. The spurious entropy generation near the inlet and at the reflection point are also common to standard structured solvers. In figs. 10 and 11 solutions on structured grids are shown, first for the NN scheme with model C and optimal choice of the triangles (fig. 10) and then the solution obtained with the standard dimensional solver (fig. 11) on the 61×21 points grid of fig. 12a. The shock capturing for the new scheme seems slightly better than for the standard solver. Comparison between other combinations of wave models and discretizations is shown in fig. 13 a-g in the form of a cut through the domain at $Y = 0.5$ and $Y = 0$ for the Mach number. In order of appearance they are : the results on the unstructured grid, model C, NN scheme (a) ; model C with the NN scheme on the structured grid with optimal choice of the diagonal (b) ; The standard solver on the same grid (c) ; the characteristic decomposition method with the NN scheme (d) on the isotropic grid of fig. 12b ; model B with the NN scheme on the iotropic grid (e) ; model C with the NN scheme on the isotropic grid (f) and model C with the N scheme on the isotropic grid (g).

The characteristic model (d) and the 6 wave model C (f) lead to monotonic results of comparable quality. However, the solution with the 6 wave model B (e) is not monotonic. This is not in contradiction with the use of a positive scheme for each wave separately, but indicates that model B is not capable of extracting the physically important upwinding directions in an oblique shock. Therefore, we will not consider model B for the further comparisons. The difference between the NN scheme compared with the N scheme for model C follows from comparing (f) with (g). The improvement obtained with the NN scheme is as expected from experience with scalar test cases[24].

Computations on a grid with optimal diagonals using model C with the NN scheme (b) compared to standard grid aligned Roe flux difference splitting on the quadrilateral grid (c) indicate that the shocks are captured in fewer cells using the present approach. These solutions are of comparable quality of the results obtained on the unstructured grid (a). Fig. 14 shows the convergence for fig. 13b.

For the supersonic channel, the iso Mach lines of fig. 15 using the NN scheme with model C are again superimposed on an almost uniform unstructured grid of 1977 vertices. The bump is shifted a bit towards the entry of the channel with respect to the standard configuration to catch a bit of the fourth reflected shock. On the structured grid using optimal diagonals, NN scheme and model C (fig. 16), results are compared with the standard grid aligned Roe flux difference splitter (fig. 17) on a grid of 63×33 points shown in fig. 18. The multidimensional solver shows slightly better definition of the first reflected shock than the standard solver. This is confirned by a cut of the value of the Mach number on the lower wall for the three cases (fig. 19).

Considering next the transonic GAMM channel, on the structured 80×33 grid of fig. 20, a comparison is made between the present approach (model C, NN scheme, optimal diagonals) (fig. 21) and grid aligned Roe FDS on the same mesh, using the quadrilaterals only (fig. 22). The boundary conditions for both solvers differ, which may explain the difference of the Mach number in the two solutions. The performance is not as good as for the fully supersonic flow test cases, although the essential phenomena of the flow appear in the solution, including a noticable reexpansion after the shock. The iso Mach lines are less smooth, an observation confirmed by a cut over the lower wall (fig. 23).

Finally, a preliminar result for the iso Mach lines in a fully subsonic flow in the same channel is shown in fig. 24, obtained with model C and the NN scheme. The deterioration of the quality of the solution already apparent in fig. 21 has progressed, resulting in a solution which lacks the symmetry expected for a fully subsonic flow. The iso pressure lines (fig. 25) however are much more symmetric, which is confirmed by a cut of the pressure on the lower wall (fig. 26). Again the boundary treatment gives Mach numbers slightly lower than those for for the structured dimensional solver. The unstructured grid of fig. 27 contained 3092 vertices with a less regular shape due to the increased density on the lower wall. The code does not suffer from a lack of robustness however. Local timestepping with a CFL of 0.8 has always been possible with model C and the NN scheme, but convergence tends to stagnate at a level where the density updates are about four orders of magnitude lower than the density itself.

A general conclusion from the numerical results shown is that at present the method described performs well for supersonic flows, where the numerical results are comparable to- or better than those from standard solvers. The influence of the wave model is large. Model B lacks monotonicity, while the characteristic decomposition method fails to work under subsonic conditions. Focussing on model C with the NN scheme, shock resolution is good, and sometimes better than what can be obtained with standard solvers. The solutions for lower Mach numbers are of preliminary character.

6. Conclusion.

In this paper we have presented a coherent overview of the concepts needed to generalize Roe's one-dimensional approximate Riemann solver to multidimensional flow in a way which does not rely on dimensional splitting. Finding the relevant waves and applying a correct upwind discretization turns out to be considerably more difficult than in 1D. On the other hand, a conservative parameter-vector linearization in 2D and 3D is conceptually similar to the 1D development and poses no problems, provided that triangular cells are used in 2D, and tetrahedra in 3D.

At this development stage the computational results are still to be considered preliminar, in particular for subsonic flow problems. Evidently, more work remains to be done on wave modeling and boundary conditions, while the linearization and scalar distribution schemes are satisfactory from the theoretical point of view. Nevertheless, model C shows improvements in shock capturing compared to standard solvers, especially on unstructured grids. On structured grids, the gain is present in case flow phenomena are not aligned with the grid.

Additional to theoretical considerations and the gain in performance shown here compared to standard 2D and 3D solvers, the decomposition in scalar waves opens also the way for local characteristic timestepping[30] and optimal multistage timestepping for efficient multigrid smoothing[31]. The compact stencils may prove convenient for massive parallelization and implicit schemes.

Acknowledgements.

The work at VKI was supported by the Commission of the European Community under Contract AERO-0003-C in Area 5 (Aeronautics) of the BRITE/EURAM Programme (1989-1993). The authors acknowledge Giuseppe Pascazio and Marcello Manna for their contribution in running the testcases.

References

1 P.L. Roe : Discrete Models for the Numerical analysis of Time-Dependent Multidimensional Gas Dynamics. J. Comp. Phys. 63, 458-476 (1986)

2 H. Deconinck, C Hirsch, J. Peuteman : Characteristic Decomposition Methods for the Multidimensional Euler Equations. Lecture Notes in Physics 264, pp 216-221, Springer, 1986

3 Ch. Hirsch, C. Lacor : Upwind Algorithms Based on a Diagonalization of the Multidimensional Euler Equations. AIAA 89-1958, June 13-15, 1989, Buffalo, New York.

4 K.G. Powell, B. van Leer : A Genuinely Multi-Dimensional Upwind Cell-vertex Scheme for the Euler Equations. AIAA 89-0095, January 9-12, 1989, Reno, Nevada

5 H. Deconinck : Upwind Methods and Multidimensional Splittings for the Euler Equations. Von Karman Institute Lecture Series 1991-01 'Computational Fluid Dynamics', February 1991

6 D.W. Levy, K.G. Powell and B. van Leer : An Implementation of a Grid-Independent Upwind Scheme for the Euler Equations AIAA 89-1931-CP, June 13-15, 1989, Buffalo, NY.

7 K.G. Powell, B. van Leer and P.L. Roe : Towards a Genuinely Multi-Dimensional Upwind Scheme. von Karman Institute Lecture Series 1990-04 'Computational Fluid Dynamics', March 1990

8 C.L. Rumsey, B. van Leer and P.L. Roe : A Grid-Independent Approximate Riemann Solver with Applications to the Euler and Navier-Stokes Equations. University of Michigan, Ann Arbor, MI, USA

9 K.G. Powell, B. van Leer and P.L. Roe : Multi-Dimensional Cell-Vertex Schemes for Convection. Dept. of Aerospace Engineering, University of Michigan, Ann Arbor, Michigan, USA

10 D. Kröner : Numerical schemes for the Euler equations in two space dimensions without dimensional splitting. Proceedings of the 2^{nd} conference on hyperbolic problems.

11 P.M. Goorjian : A streamwise upwind algorithm for the Euler ans Navier-Stokes equations applied to transonic flows. Proceedings of the ICNMFD conference, Oxford, 1988

12 B. Koren : Low-Diffusion Rotated Upwind Schemes, Multigrid and Defect Correction for Steady, Multi-Dimensional Euler Flows. International Series of Numerical Mathematics, Vol. 98. Birkhauser Verlag, 1991

13 P.W. Hemker, B. Koren : Efficient Multi-dimensional Upwinding for the Steady Euler Equations. CWI Report NM-R9107, 1991

14 R. Struijs, H. Deconinck : Multidimensional Upwind Schemes for the Euler Equations Using Fluctuation Distribution on a Grid Consisting of Triangles. 8th GAMM Conference on Numerical Methods in Fluid Mechanics, Delft University of Technology, September 27-29, 1989.

15 P.L. Roe : The Use of the Riemann Problem in Finite-Difference schemes. Lecture Notes in Physics, vol 141, eds. W.C. Reynolds, R.W. MacCormack. Springer, 1981 ICNMFD

16 P.L. Roe : Fluctuations and signals, a framework for numerical evolution problems. Numerical Methods for Fluid Dynamics II; eds. K.W. Morton, M.J. Baines , pp 219-257, Academic Press, 1982.

17 P.L. Roe : Approximate Riemann Solvers, Parameter Vectors and Difference Schemes. J. Comp. Phys. 43, 357-372, 1981

18 P. De Palma, H. Deconinck and R. Struijs : Investigation of Roe's 2D wave decomposition models for the Euler equations. Von Karman Institute Technical Note 172, july 1990

19 P.L. Roe, R. Struijs and H. Deconinck : A conservative linearisation of the multidimensional Euler equations. Submitted to J. Comp. Phys 1991

20 P.L. Roe : A Basis for Upwind Differencing of the Two-Dimensional Unsteady Euler Equations. Numerical Methods for Fluid Dynamics II, pp 55-80, eds. K.W. Morton, M.J. Baines Oxford University Press, 1986

21 P.L. Roe : Linear Advection Schemes on Triangular Meshes. Cranfield Institute of Technology CoA Report No 8720, Cranfield, Bedford, U.K., November 1987

22 P.L. Roe, H. Deconinck, R. Struijs : Recent Progress in Multidimensional Upwinding. Proceedings ICNMFD Conf., Oxford, July 1990

23 P.L. Roe : Numerical Algorithms for the Linear Wave Equation. Royal Aircraft Establishment Technical Report 81047, 1981

24 R. Struijs, H. Deconinck, P.L. Roe : Fluctuation Splitting Schemes for the 2D Euler Equations. von Karman Institute Lecture Series 1991-01 'Computational Fluid Dynamics', February 1991

25 P.L. Roe, H. Deconinck and R. Struijs : Genuinely two-dimensional computation of scalar conservation laws. To be submitted to J. Comp. Physics, 1991.

26 S. Spekreijse : Multigrid Solution of the Steady Euler Equations. Ph.D. Thesis, Amsterdam, 1987.

27 D. Sidilkover : Numerical solution to steady-state problems with discontinuities. Ph.D. Thesis, The Weizmann Institute of Science, 1989.

28 J.G. Rice, R.J. Schnipke : A monotone streamline upwind finite element for convection dominated flows. Comp. Meth. in Appl. Mech. and Eng., Vol 48, p 313-327, 1985

29 T.J.R. Hughes, M. Mallet, A. Mizukami : A new finite-element formulation for computational fluid dynamics. II, beyond SUPG. Comp. Meth. Appl. Mech. and Eng., Vol 84, No 3, 1986.

30 B. Van Leer, B-H. Tai, K.H. Powell : Design of optimally smoothing multi-stage schemes for the Euler equations. AIAA 89-1933-CP, 1989

31 L.A. Catalano, H. Deconinck and M. Napolitano : Optimal multi-stage schemes for multigrid smoothing of two-dimensional advection operators. Proc. 5th Copper Mountain conference on multigrid methods, 1991.

32 M. Manna : A 3-D high resolution upwind finite volume Euler solver. VKI Tech. Note, 1991

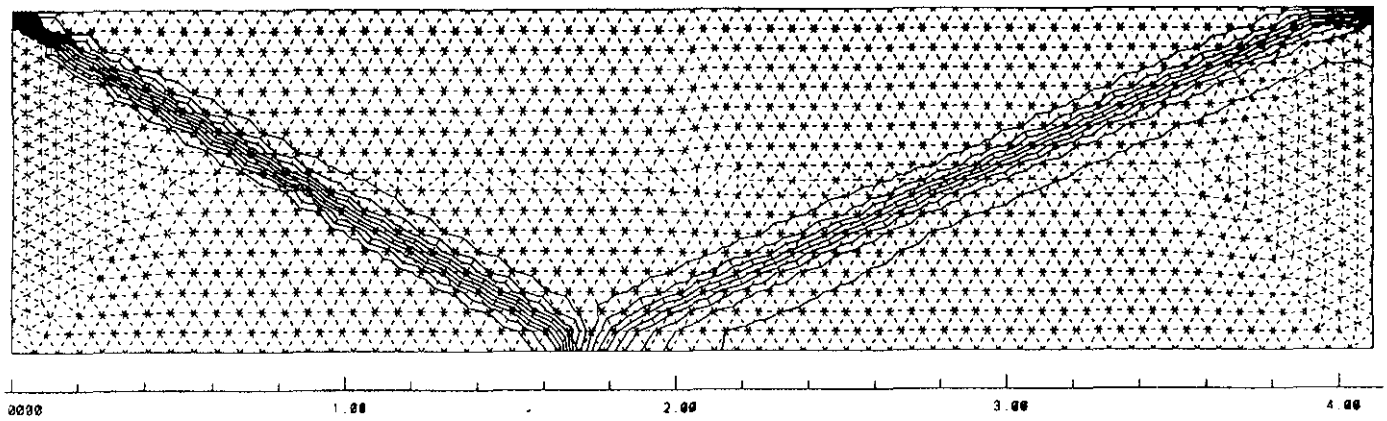

Fig. 8. Oblique shock reflection. Iso Mach lines superimposed on the unstructured grid for model C with the NN scheme. Increment = .05 The grid has 1235 vertices.

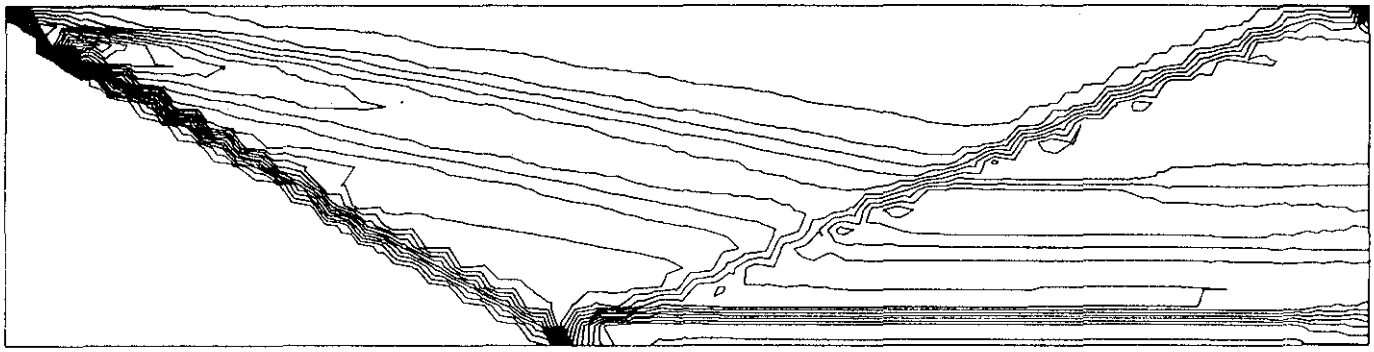

Fig. 9. As fig. 8 ; Iso-entropy lines. Increment = .005

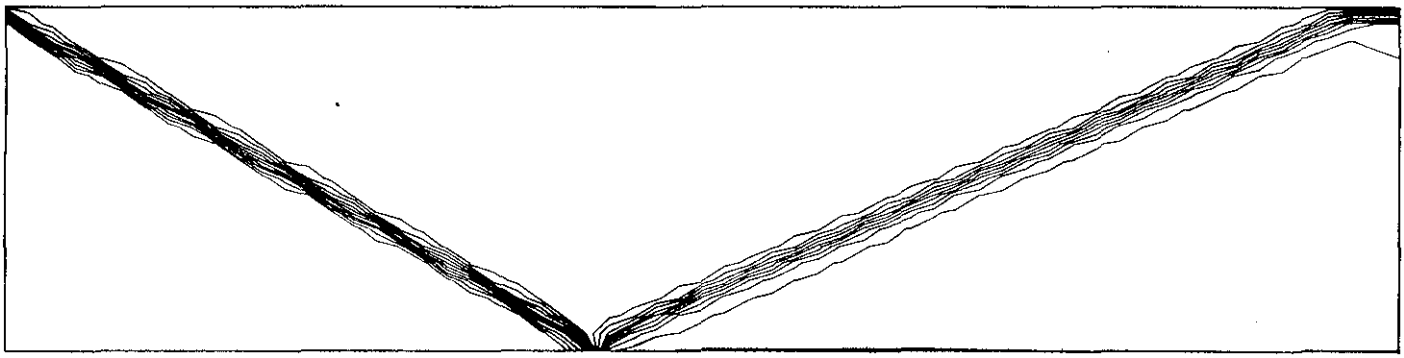

Fig. 10. Oblique shock reflection on structured grid. Iso Mach lines for model C with the NN scheme and optimal choice of the diagonals. Increment = .05 The grid has $61 \times 21 = 1281$ vertices.

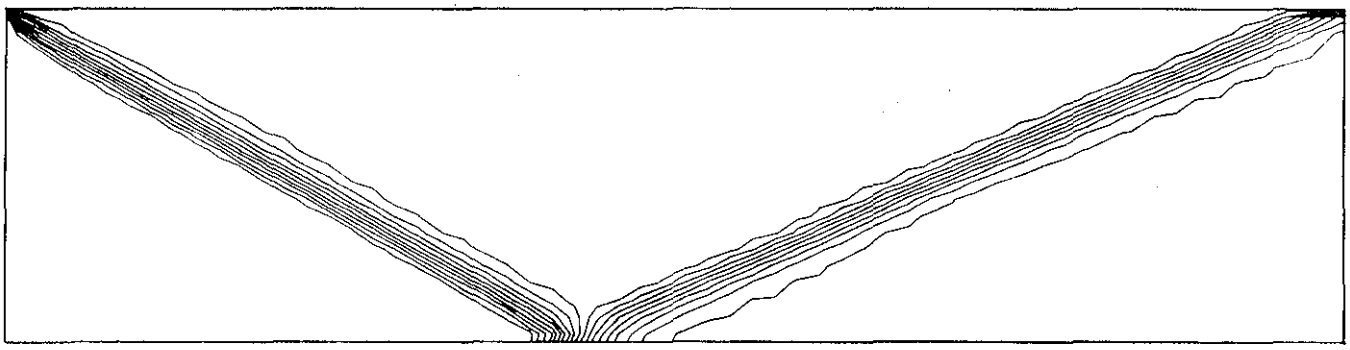

Fig. 11. Oblique shock reflection on structured grid. Iso Mach lines for a grid aligned cell centered finite volume Roe flux difference splitter with $\kappa = \frac{1}{3}$. Increment .05 The grid has $62 \times 22 - 1364$ unknowns.

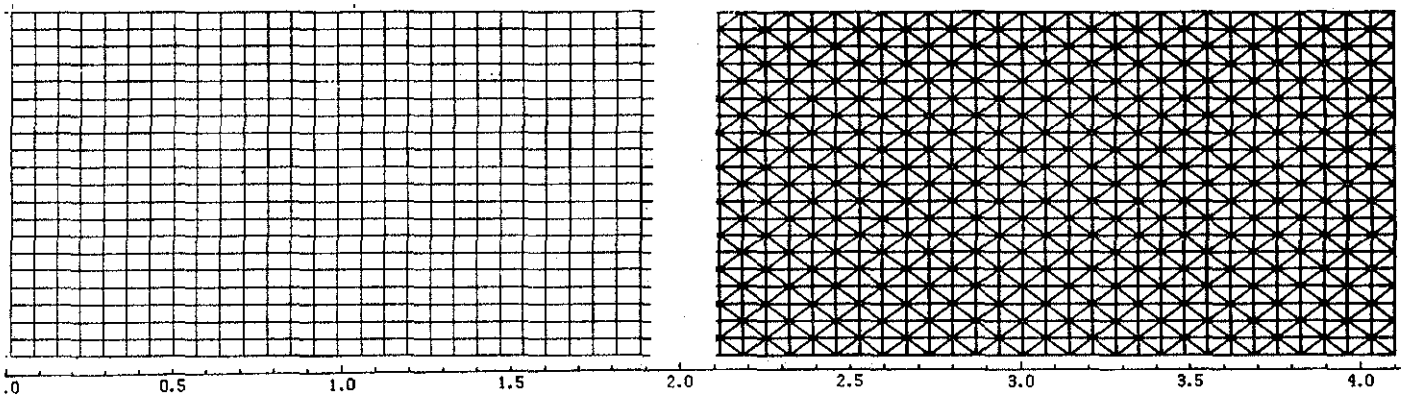

Fig. 12. Parts of the grids used for the standard solver (a), and of the isotropic grid for the multidimensional solver (b).

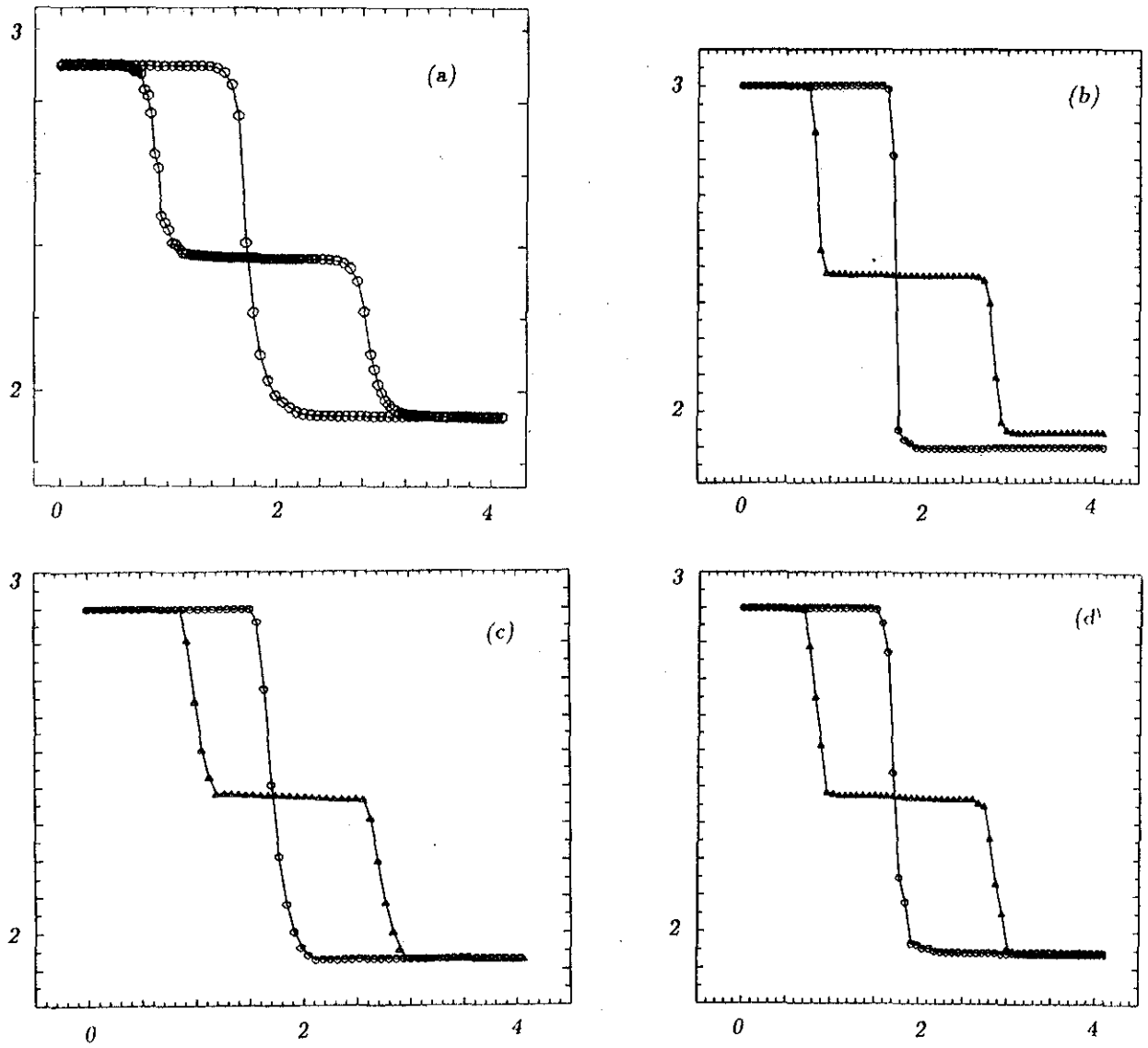

Fig. 13 (a)-(d). Value of the Mach number along lines $Y = 0.5$ and $Y = 0$ for (a) model C with the NN scheme on the unstructured grid, (b) model C with the NN scheme on the structured grid using optimal diagonals, (c) the standard solver on the structured grid, (d) the characteristic decomposition used with the NN scheme on the isotropic grid.

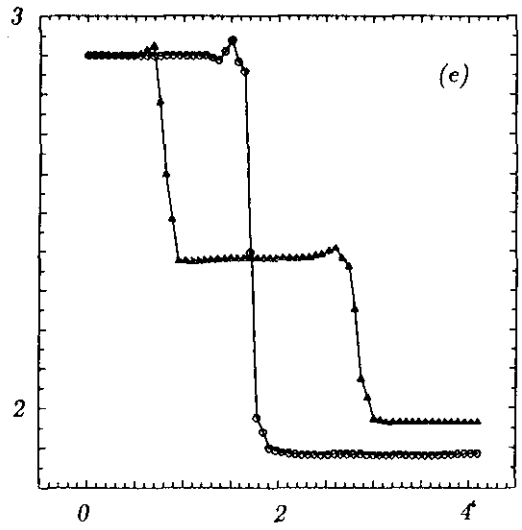

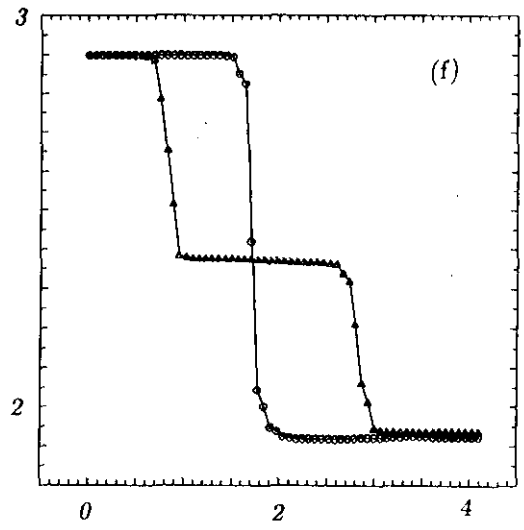

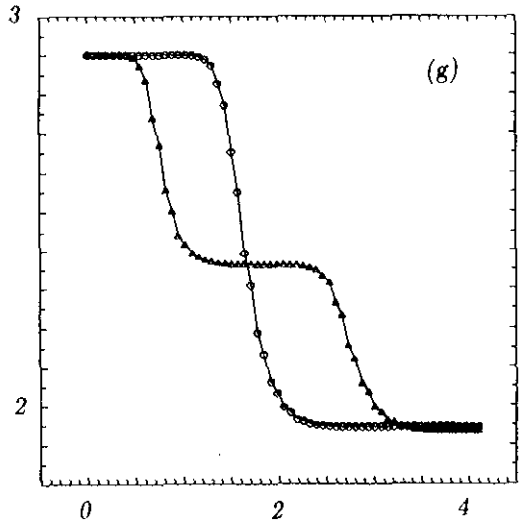

Fig. 13 (e)-(g). Value of the Mach number along lines $Y = 0.5$ and $Y = 0$ for (e) model B with the NN scheme on the isotropic grid, (f) model C with the NN scheme on the isotropic grid, (g) model C with the N scheme on the isotropic grid.

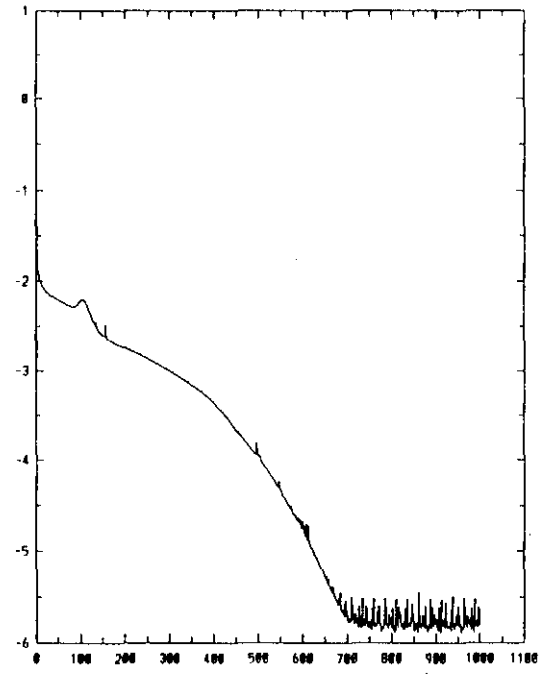

Fig. 14. Convergence history for the solution of fig. 13 b.

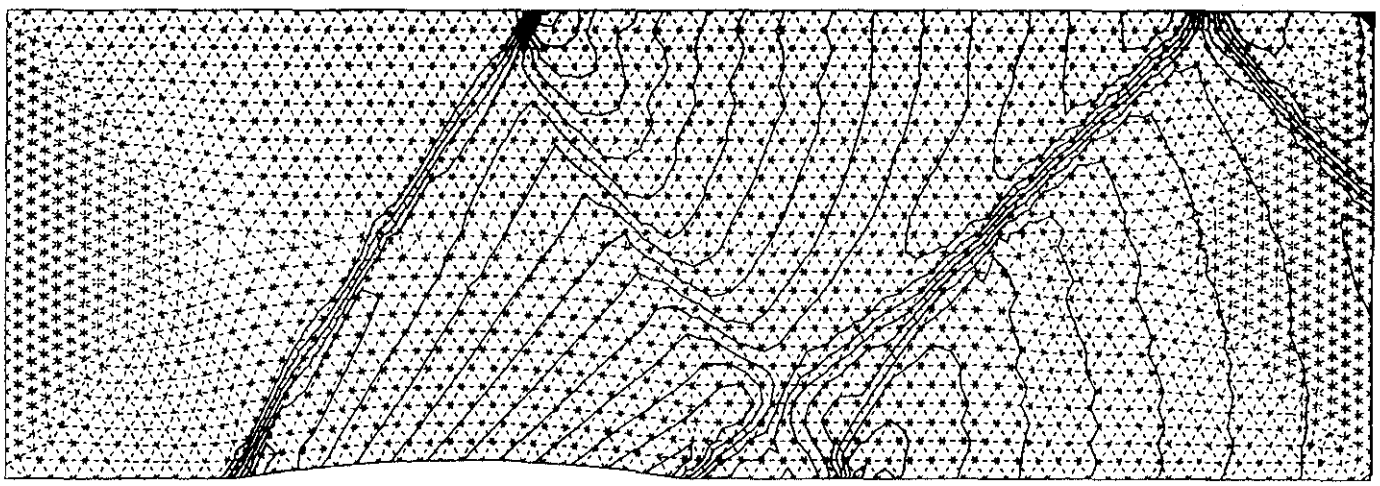

Fig. 15. Supersonic channel flow with inlet Mach number of 1.4. Isolines of the Mach number with an increment of 0.05 for Model C with the NN scheme superimposed on the unstructured grid.

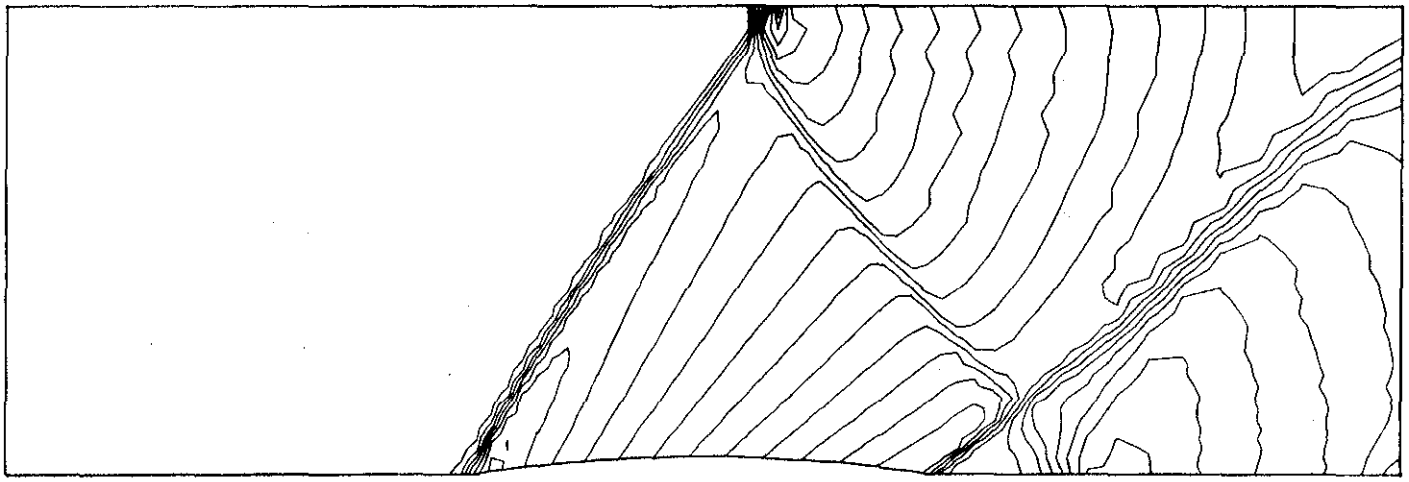

Fig. 16. As fig. 15, but on the structured grid of fig. 18 with the optimal choice of the diagonal.

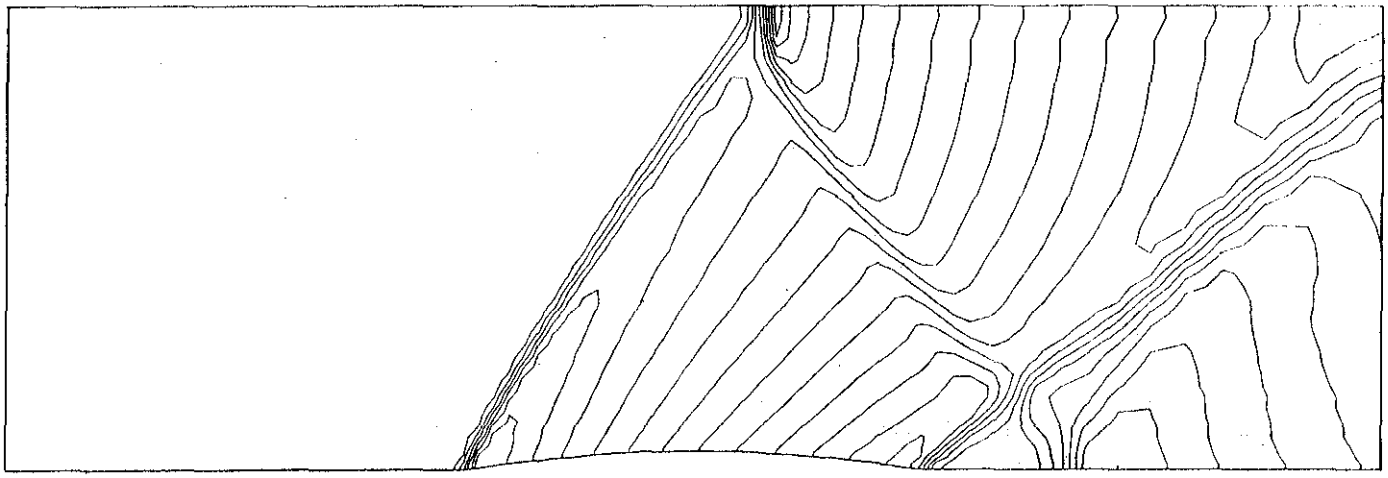

Fig. 17. Iso Mach lines for the standard solver on the grid of fig. 18.

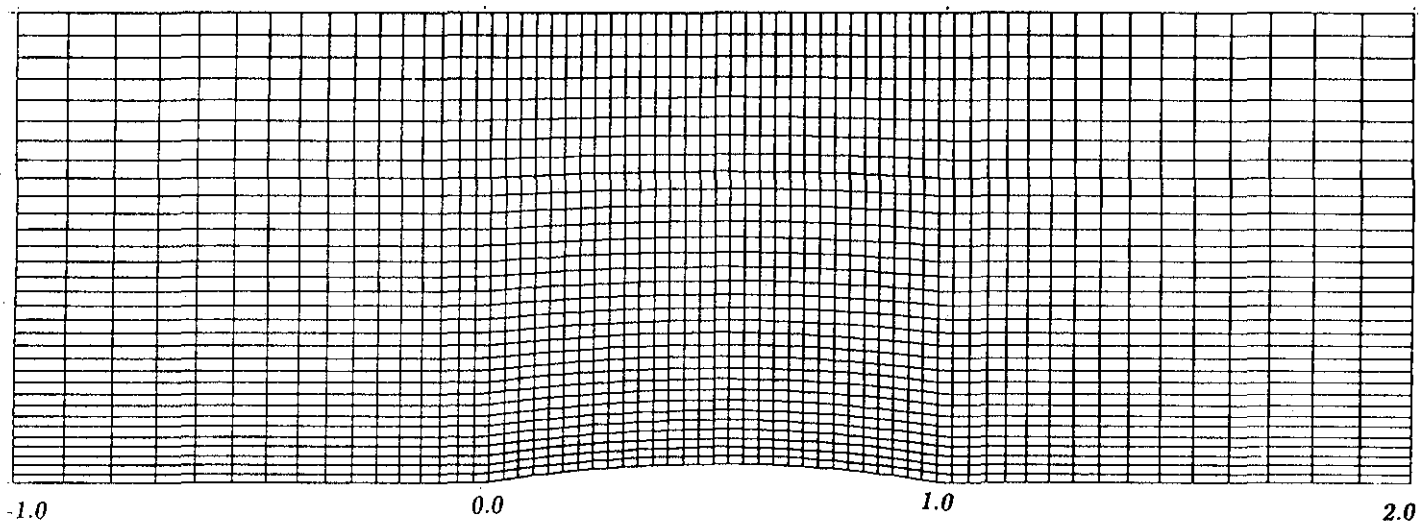

Fig. 18. The structured grid for the supersonic channel flow test case.

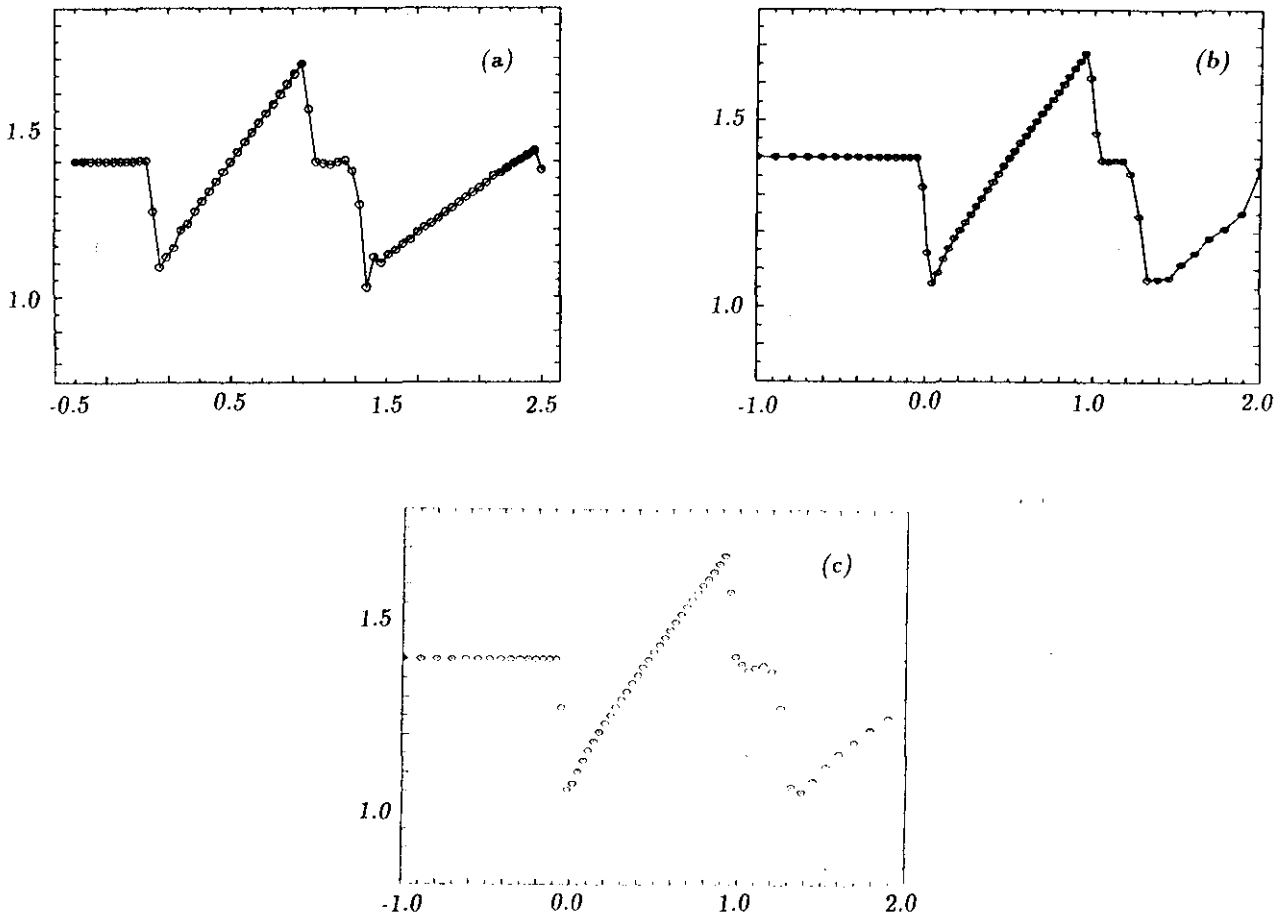

Fig. 19. The value of the Mach number on the lower wall for the supersonic channel flow for the solutions of figs. 15-17 respectively in (a)-(c).

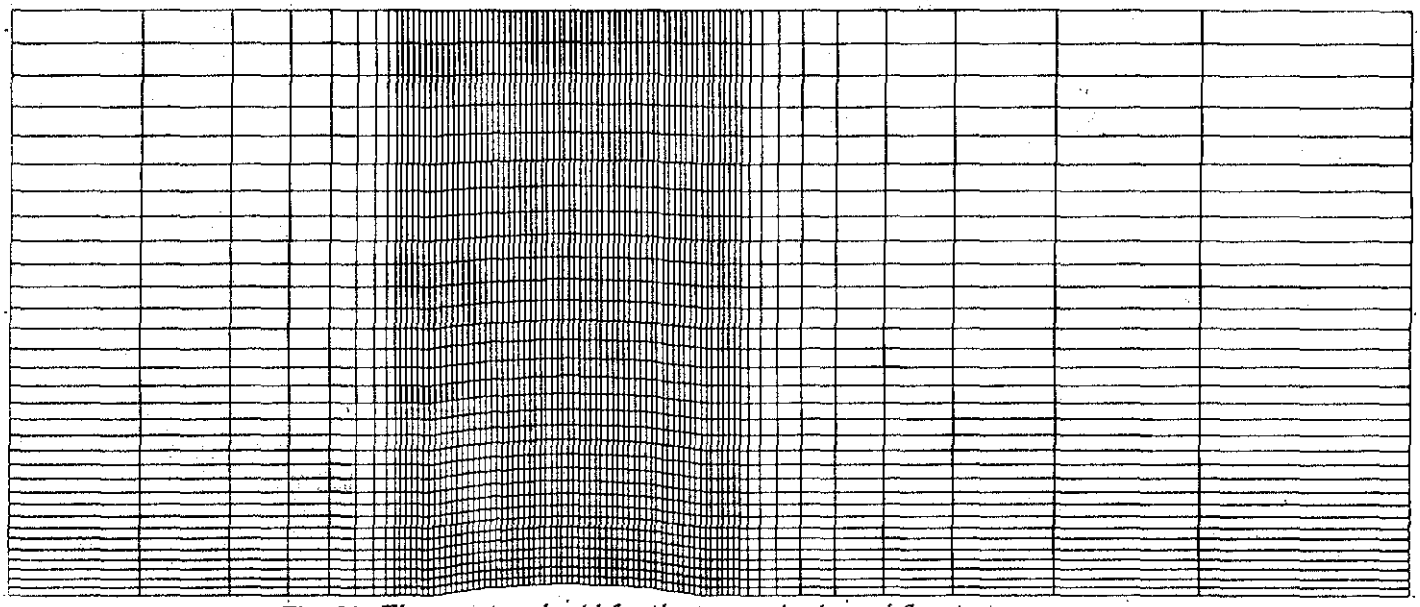

Fig. 20. The structured grid for the transonic channel flow test case.

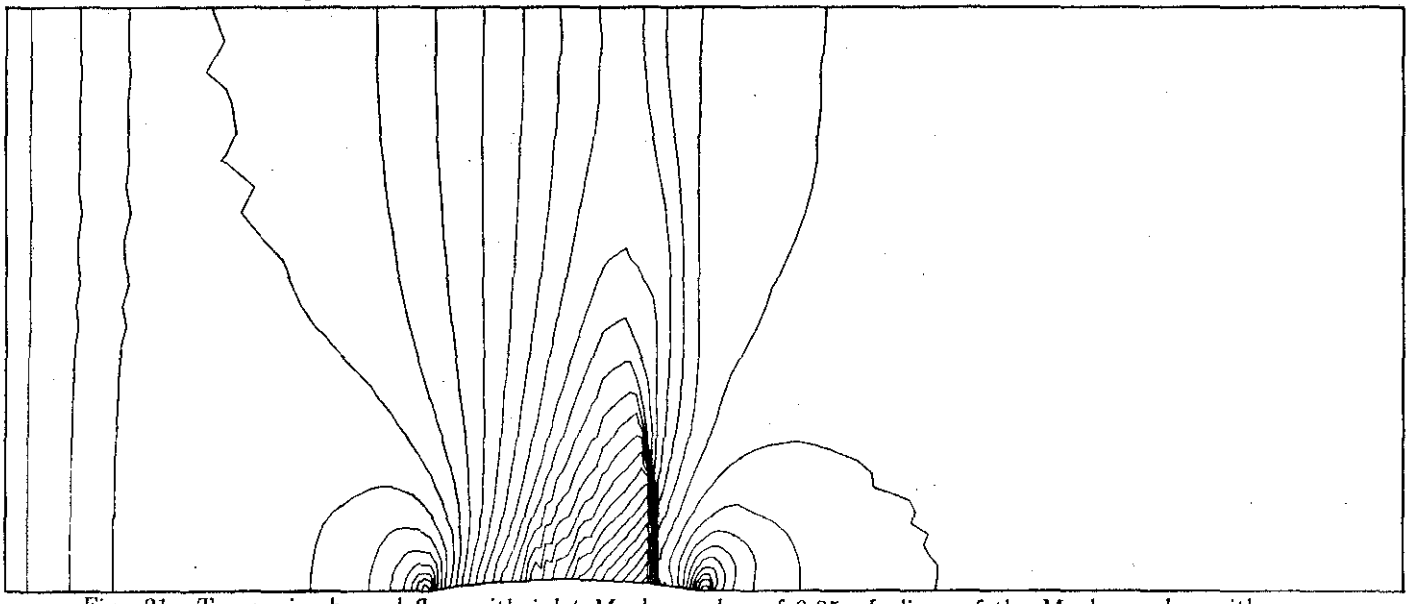

Fig. 21. Transonic channel flow with inlet Mach number of 0.85. Isolines of the Mach number with an increment of 0.05 for Model C with the NN scheme on the structured grid of fig. 20 with the optimal choice of the diagonal.

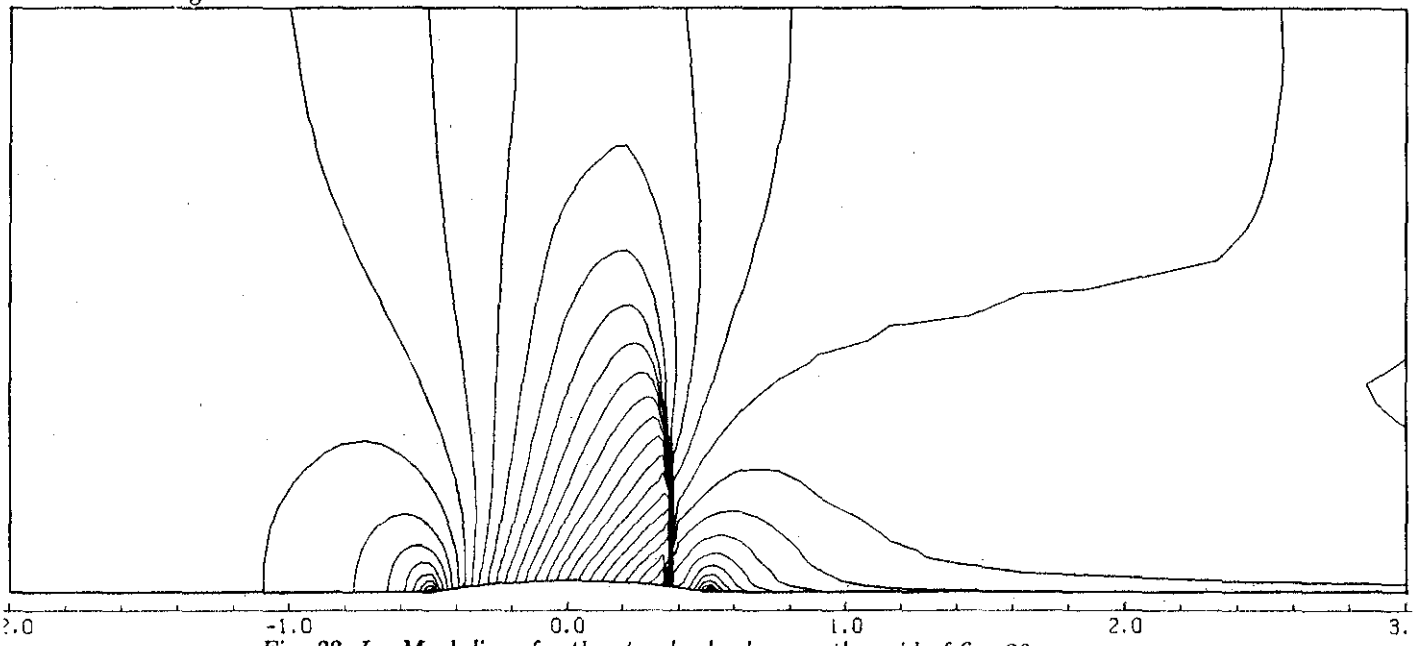

Fig. 22. Iso Mach lines for the standard solver on the grid of fig. 20.

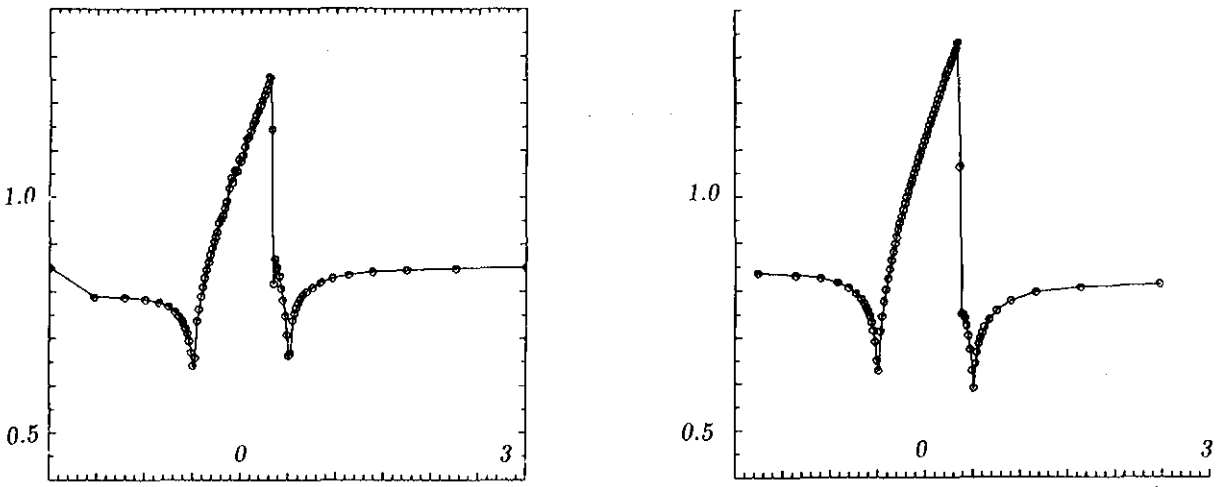

Fig. 23. The value of the Mach number on the lower wall for the transonic channel flow for the solutions of figs. 21 and 22 respectively in (a) and (b).

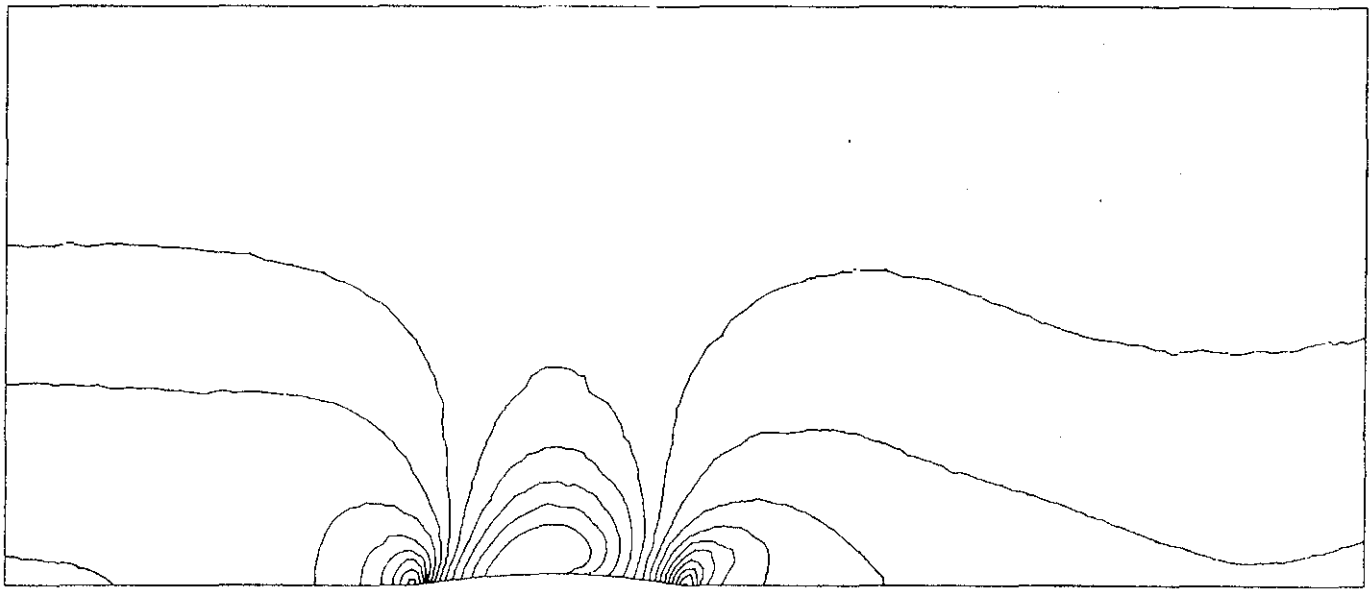

Fig. 24. Subsonic channel flow with inlet Mach number of 0.6. Iso lines of the Mach number with an increment of 0.01 for Model C with the NN scheme on the unstructured grid of fig. 27.

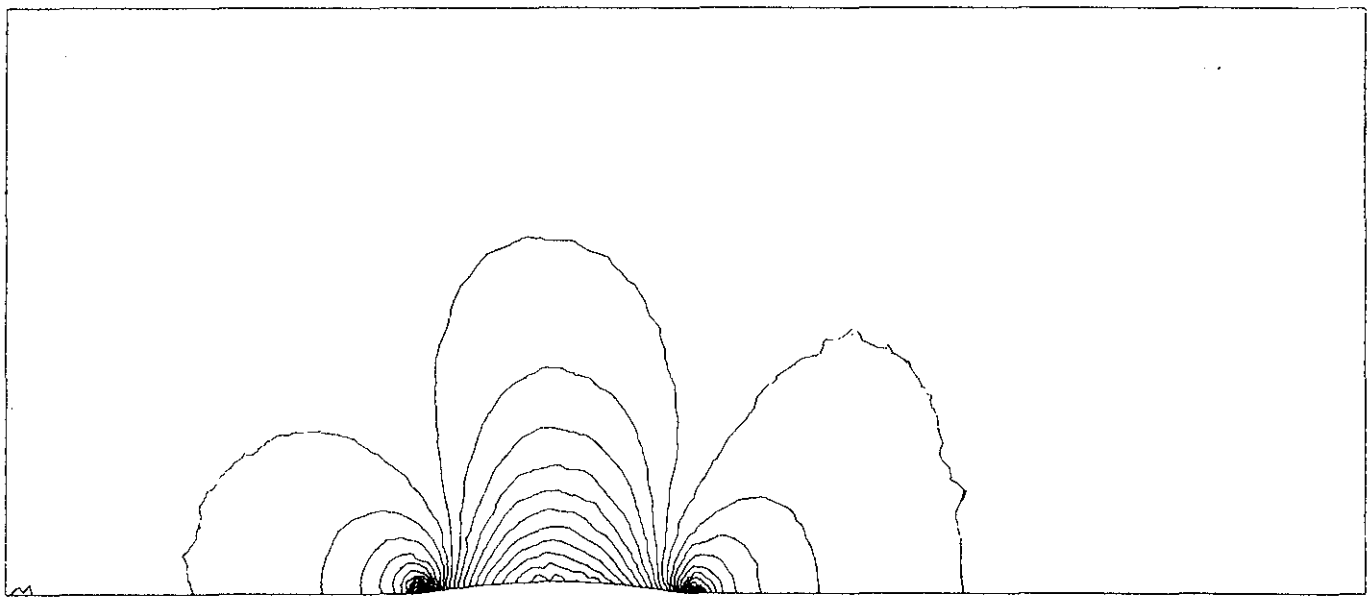

Fig. 25. As fig. 24 ; Iso lines for the pressure with an increment of 1000. (P_T 10^5).

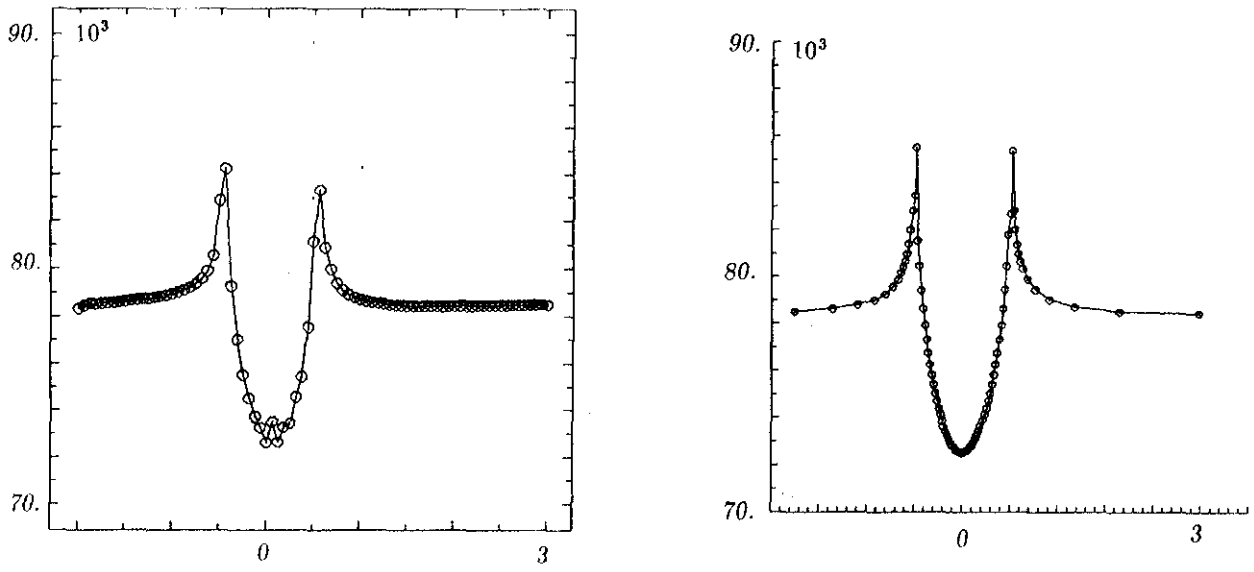

Fig. 26. The value of the pressure on the lower wall for the subsonic channel flow for the multidimensional solver (fig. 25) and the standard solver on a 80×33 *grid clustered towards the center, respectively in (a) and (b).*

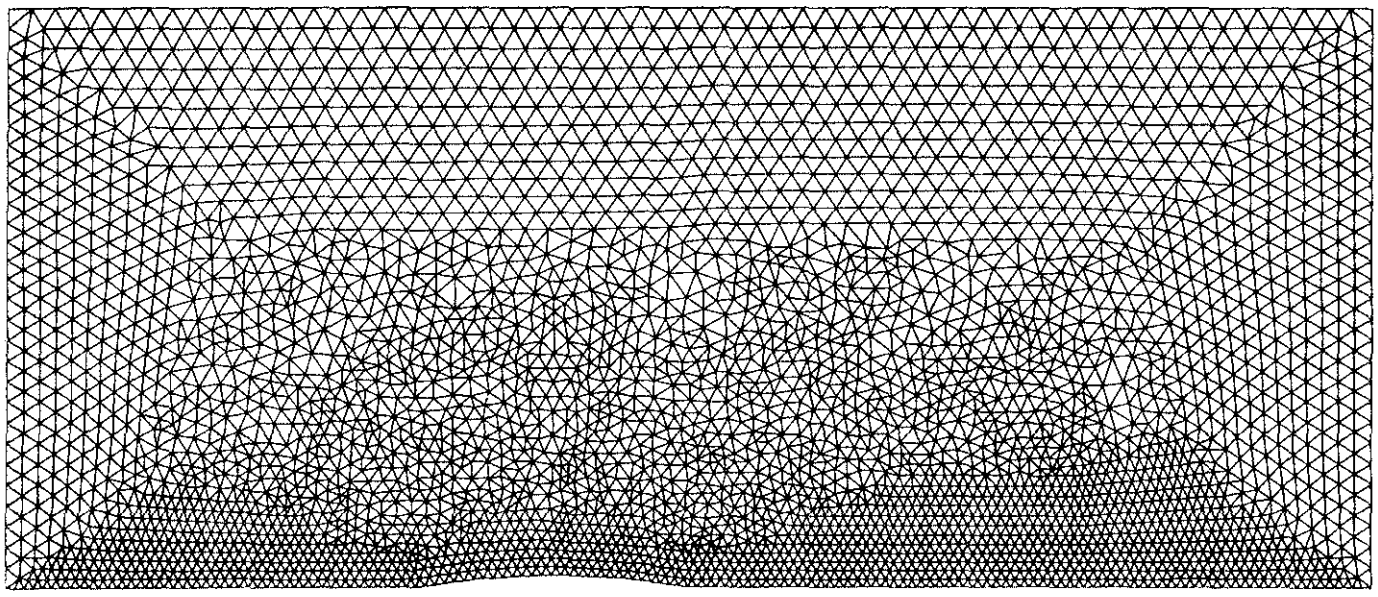

Fig. 27. Unstructured grid with 3092 vertices used for the computations of fig. 24, 25 and 26(a).